

1 **Shoreline and Land Use Land Cover Changes along the 2004 tsunami-**  
2 **affected South Andaman Coast: Understanding Changing Hazard**  
3 **Susceptibility**

4 Vikas Ghadamode<sup>1,2</sup>, Aruna Kumari Kondarathi<sup>1</sup>, Anand K Pandey<sup>1,2</sup> Kirti Srivastava<sup>1</sup>

5 1. CSIR- National Geophysical Research Institute, Hyderabad, 500007 India.

6 2. Academy of Scientific and Innovative Research (AcSIR), Ghaziabad 201002, India.

7

8 § Corresponding author: Email address: [akpandey@ngri.res.in](mailto:akpandey@ngri.res.in)

9 *Tel: +91-40-27012416*

10

11

Deleted: K.

Deleted: Aruna<sup>1</sup>

14 **Abstract**

15 The 2004 tsunami affected the South Andaman coast, experiencing dynamic changes in the  
16 coastal geomorphology, making the region vulnerable. We focus on pre-and post-tsunami  
17 shoreline and Land Use Land Cover changes for 2004, 2005, and 2022 to analyse the dynamic  
18 change in hazard. We used GEBCO bathymetry data to calculate Run-up (m), arrival times  
19 (Min), and inundation (m) at a few locations using three tsunamigenic earthquake source  
20 parameters, namely the 2004-Sumatra, 1941-North Andaman, and 1881-Car Nicobar  
21 earthquakes. The Digital Shoreline Analysis System is used for the shoreline change estimates.  
22 The Landsat data is used to calculate shoreline and Land Use Land Cover (LULC) change in  
23 five classes, namely Built-Up Areas, Forests, Inundation areas, Croplands, and water bodies  
24 during the above period. We examine the correlation between the LULC changes and the  
25 dynamic change in shoreline due to population flux, infrastructural growth, and Gross State  
26 Domestic Product growth. India industry estimates the Andaman & Nicobar Islands losses  
27 exceed INR 10 billion during 2004, which would see a five-fold increase in economic loss due  
28 to a doubling of built-up area, a three-fold increase in tourist inflow, and a population density  
29 growth. The unsustainable decline in the forest cover, mangroves, and cropland would affect  
30 sustainability during a disaster despite coastal safety measures.

31 **Keywords: Geomorphology, Land use Land cover, Shoreline, Tsunami, Remote sensing**

32

Deleted: -

Deleted: the period

Deleted: 13 different

Deleted: the 2004 Sumatra Earthquake

Deleted: that

38 **1. Introduction:**

39 The Coastal shorelines are dynamic and highly vulnerable to erosion and accretion caused  
40 by hydrodynamic, tectonic, geomorphic, and climate forcing, including tsunamis, cyclones,  
41 flooding, storm surges, wave action, wind and tide changes, and sea level variations (Nayak  
42 2002; Boak & Turner 2005; Kumar et al., 2010; Mukhopadhyay et al., 2011). In addition to  
43 natural coastal processes, coastal resources are constantly under stress due to anthropogenic  
44 activities, such as industrialization, port construction, beach sand mining, garbage dumping,  
45 urbanization, trade, tourism, and recreational activities, which significantly impact the  
46 shoreline and results into damage to natural ecosystems (Yi et al., 2018; Davis, 2019). It is  
47 important to regularly monitor spatiotemporal along shorelines, Land use / Land Cover  
48 (LULC), and geomorphic features (Moran, 2003; Cooper et al., 2004; Scheffers et al., 2005;  
49 Jayakumar & Malarvannan, 2016). Several studies have analyzed various coastal processes,  
50 including mapping, shoreline change, LULC change detection, and analysis of  
51 geomorphological landforms using satellite data. The temporal multispectral satellite data  
52 allow for the identification of regions undergoing erosion or accretion change (Misra and  
53 Balaji, 2015; Kumari et al., 2012; Tonisso et al., 2012; Murali et al., 2013; Sudha Rani et al.,  
54 2015; Rowland et al., 2022; Thiéblemont et al., 2021). The M 9.3 undersea earthquake on  
55 December 26, 2004, near the coast of Sumatra, Indonesia, triggered the Indian Ocean tsunami  
56 and caused massive destruction of the coastal ecosystem in the Andaman region (Sheth et al.,  
57 2006; Ramalanjaona, 2011). The shoreline and geomorphological changes of the 2004 Sumatra  
58 tsunami were analyzed using statistical techniques on remote sensing data (Kumari et al., 2012;  
59 Yuvaraj et al., 2014; Yunus and Narayana, 2015; Yunus et al., 2016).

60 Since the 2004 tsunami, the Andaman and Nicobar Islands have experienced notable  
61 population growth, infrastructural development, and flourishing tourism activities over the past  
62 decade (Yuvaraj et al., 2014). The development is profound in the south Andaman region. This

Deleted: .

Deleted: .

Deleted: .

Deleted: spatio-temporal

Deleted: )

Deleted: .

Deleted: .

Deleted: been conducted to analyse

Deleted: the

Deleted: of

Deleted: .

Deleted: .

Deleted: .

Deleted: .

Deleted: .

Deleted: .

Deleted: , Thiéblemont

Deleted: .

Deleted: Indian Ocean tsunami of December 26, 2004 was triggered by a magnitude

Deleted: Caused

Deleted: .

Deleted: Using remote sensing data and statistical techniques the

Deleted: & geomorphology

Deleted: caused by

Deleted: examined (Mouat and Lancaster 1996; Saraf and Choudhary, 1999; Reid et al. 2000; Chen 2002; Weng 2002; Siddiqui and Maajid 2004; Mujabar and Chandrasekhar 2011;

Deleted: .

Deleted: Tonisso et al. 2012; Jangir et al. 2014;

Deleted: .

Deleted: Tsunami

Deleted: remarkable

Deleted: progress

Deleted: .

99 is a cause of concern for the tsunami vulnerability as the region is prone to large earthquakes  
100 and is a seismo-tectonically active plate boundary. In this study, we Compute Tsunami arrival  
101 times, run-up heights, and inundation extent along the south Andaman region. We also  
102 analyzed dynamic vulnerability using temporal and spatial changes in shoreline and LULC for  
103 the tsunami-affected areas (Velmurugan et al., 2006; Ghadamode et al., 2022). The analysis  
104 covers three time periods: 2004 (pre-tsunami), 2005 (post-tsunami), and 2022 (current state) of  
105 shoreline changes using multi-temporal Landsat data employing the End Point Rate (EPR) and  
106 Net Shoreline Movement (NSM) methods (Himmelstoss et al., 2021) and LULC changes. A  
107 relationship between LULC changes and vital socioeconomic factors such as population  
108 dynamics, tourism trends, and the Gross State Domestic Product (GSDP) is established to  
109 assess the potential future impacts of tsunamis in the region. The results would provide  
110 actionable insights to the policymakers, coastal planners, and stakeholders in disaster  
111 management and sustainable coastal development.

## 112 2. Study Area

113 South Andaman region, with ~1,262 km<sup>2</sup> area and a 413 km coastline, is the  
114 southernmost island of the Great Andaman, where most of the Andaman Island's population  
115 and infrastructure are centered. As per the 2011 Indian census, South Andaman has a  
116 population of 238,142 people, which increased to 266,900 in 2021 (estimate based on  
117 www.census2011.co.in). The most habitable areas in the eastern part of South Andaman are  
118 located on low lands at bay heads in addition to the higher slopes bordering bays and coastal  
119 flat lands (Ghosh et al., 2004), which experienced devastation and losses during the 2004  
120 Tsunami (Fig. 1). We selected 13 locations, namely South Point in Port Blair, Rutland Island,  
121 Corbyn's Cove Beach, Madhuban Bay, Brichgunj, Chidiyatopu, Thirupatti Temple,  
122 Wandoorjetty, Bamboo Flat, Potatang, Shoal Bay, Radha Nagar, and Govinda Nagar (Fig. 1)  
123 for vulnerability assessment in the present study.

Deleted: very

Deleted: as it

Deleted: ,

Deleted: ,

Deleted: status

Deleted: and LULC)

Deleted: to map

Deleted: extent of shoreline changes in the EPR (

Deleted: ) & NSM (NET

Deleted: ) Method

Deleted: Islands'

Deleted: centrated. According to

Deleted: . 2007). The South Andaman region

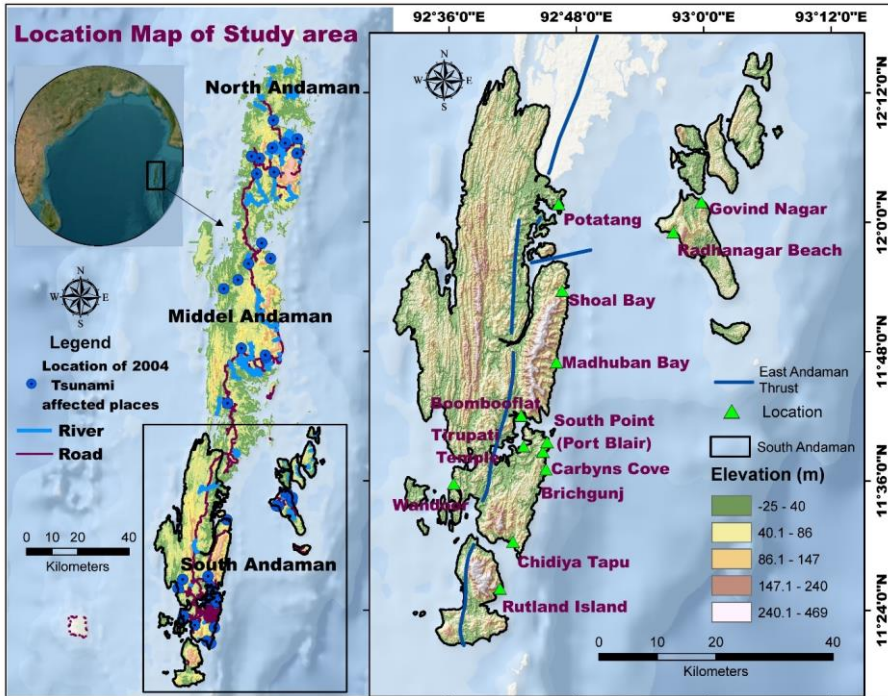
Deleted: and is vulnerable

Deleted: point

Deleted: Corbyn's cove

Deleted: flat

Deleted: bay



142

143 Figure 1 Location Map of the South Andaman Region (© Google Maps & © Google Earth).

144 The tectonic activity and weathering processes have influenced the region's topography  
 145 growth and evolution (Curry, 2005; Bandopadhyay and Carter, 2017). The East Andaman  
 146 Thrust, also called East Boundary Thrust, is a linear/curvilinear ~500 km long fault zone and  
 147 is the locus of ongoing convergent and crustal deformation along the Sunda-Andaman plate  
 148 boundary. This structure is pivotal in creating accretionary prisms within the outer-arc ridge of  
 149 the Andaman and Nicobar subduction zones (Fig. 1; Bhat et al., 2023).

Deleted: The region's topography is primarily influenced by

Deleted: plates.

150 The structure-bound major geomorphological features in South Andaman include hills,  
 151 valleys, beaches, mangroves, and coral reefs (Fig. 2a). The highest peak on the island is Mount  
 152 Harriet, with approximately 1,200 m (3,937 feet) (southandaman.nic.in). The north-western  
 153 and north-eastern parts of South Andaman are highly and moderately dissected, whereas the  
 154 Southern part has low dissected structural hills and valleys (Fig. 2a, b, c, and d). The upper

Moved (insertion) [1]

157 slopes of the region are covered with high dissected structural hills with dense pristine forest  
158 (Fig. 2a). The slope ranges between 0 to 44.9 degrees, with lower slopes in the coastal region  
159 mostly inhibited and undergoing rapid coastline modification and Land Use Change. The  
160 North, Northeast, and Southern portions of South Andaman have the steepest slope and relief  
161 area, while the Eastern, Southeastern, and western parts have relatively lower slopes (Fig. 2b  
162 and c). The island has a rough coastline with various bays, inlets, and headlands (Fig. 2). The  
163 Younger coastal plain is a relatively flat and low-lying area adjacent to the coastline, which is  
164 formed through the accumulation of sediments brought by the ocean (Fig. 2e). A wave-cut  
165 platform, formed by the erosive action of waves, are flat or gently sloping rock surface are  
166 found along South Point coastlines in Port Blair (Fig. 2f). These platforms can be exposed at  
167 low tide, which gradually wear away the rock over time, are unique feature of rocky coastlines.  
168 Coral reefs along the coast contribute to forming sandy beaches and barrier islands (Reguero  
169 et al., 2018). Mangrove forests are found on coasts in South Andaman Island, primarily in the  
170 brackish water and muddy sediments lagoons and tidal zone (Fig. 2g). Mangroves are crucial  
171 in stabilizing coastal ecosystems and providing habitat for various species. Wandoor, Chidya  
172 tapu, and Sippighat are some notable locations of mangrove forests in South Andaman coastal  
173 areas. The coastal plains in south Andaman are dynamic and prone to tsunamis due to their  
174 location and active plate boundary. Therefore, studying shoreline change and LULC change is  
175 especially important because of the potential impacts on local communities and ecosystems.

**Deleted:** 2d). The highest peak on the island is Mount Harriet with approximately 1,200 meters (3,937 feet) (southandaman.nic.in). The north-western part of South Andaman is highly dissected whereas the North-eastern part is moderately dissected and the Southern part is most likely low dissected structural hills and valleys (

**Deleted:** 2 a and e). The island has a rough coastline with various bays, inlets, and headlands.

**Deleted:** is a

**Deleted:** It is formed through the erosive action of waves,

**Deleted:** . These platforms can be exposed at low tide and are often a

**Deleted:** the formation of

**Moved up [1]:** The upper slopes of the region are covered with high dissected structural hills with dense pristine forest (Fig. 2a). The slope ranges between 0 to 44.9 degrees, with lower slopes in the coastal region mostly inhibited and undergoing rapid coastline modification and Land Use Change

**Deleted:** (Fig. 2 b and c). The North, Northeast, and Southern portions of South Andaman have the steepest slope and relief area, while the Eastern, Southeastern, and western parts have relatively lower slopes.

**Deleted:** , therefore

**Deleted:** due to



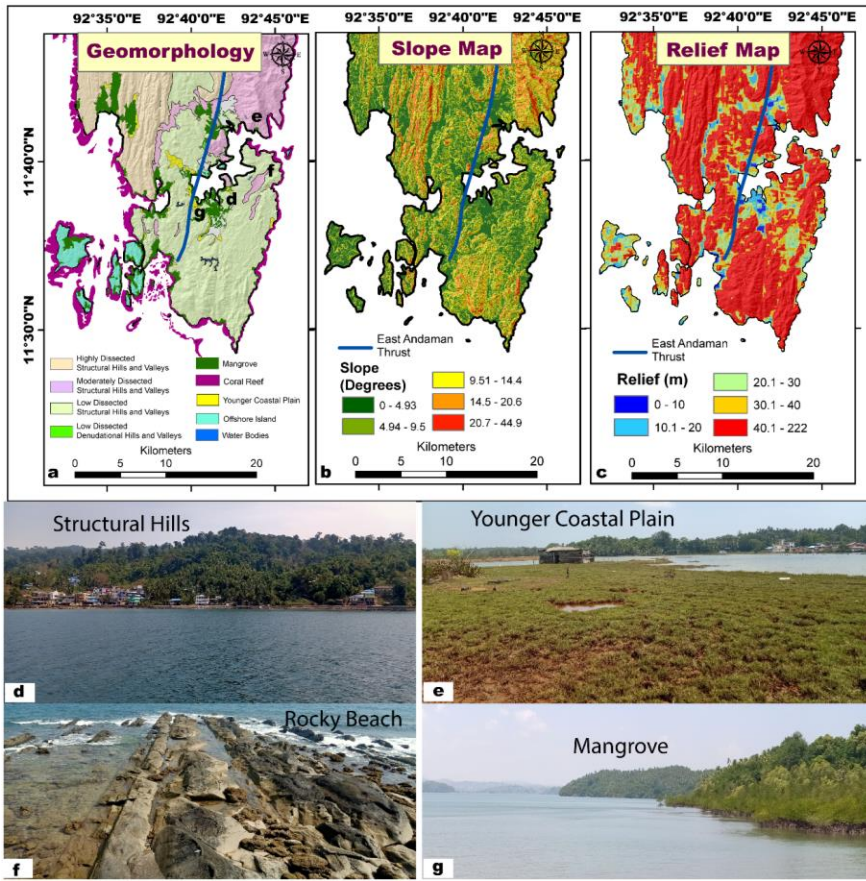
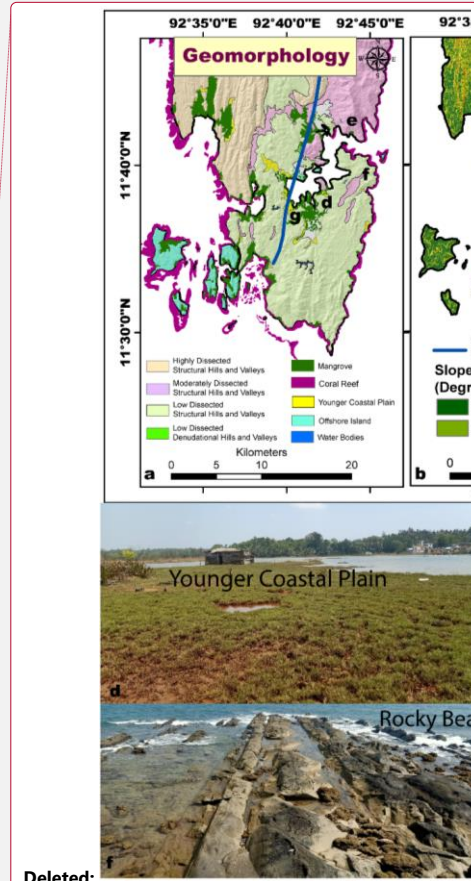


Figure 2 (a) Geomorphology, (b) Slope map, (c) Relief Map, (d) Structural Hills, (e) the younger coastal plain, (f) Rocky Beach with a wave-cut platform near south point, Port Blair, (g) Mangrove.



Deleted: , (e) Structural Hills

Deleted: To assess the vulnerability, it

Deleted: assessing

Deleted: is used

201

202

203

204

205 **3. Materials and Methods**

206 It is imperative to generate a spatial dataset that may have a bearing on the dynamic changes  
 207 to assess the vulnerability.

208 **3.1 Data Used**

209 Landsat satellite data, such as Thematic Mapper (TM) and Operational Land Imagery  
 210 (OLI) sensor for the years 2004, 2005, and 2022, is used to analyze shoreline and monitor the  
 211 LULC changes along the South Andaman coast in the present study. The Shuttle Radar

217 Topography Mission (SRTM) Digital Elevation Model (DEM) is used to prepare the study  
 218 area's slope and relief map. We used the General Bathymetry Chart of the Ocean (GEBCO) for  
 219 run-up and inundation studies along the south Andaman coastal areas (Table 1).

**Deleted:** This dataset analyzes shoreline and monitors the LULC changes along the South Andaman coast.

220 **Table 1:** Data used in the present study region

Data	Purpose	Date & Year	Resolution	Sources
GEBCO bathymetry	Inundation and Run-Up	2022	90 m	GEBCO ( <a href="https://www.gebco.net/">https://www.gebco.net/</a> )
Landsat 5 TM, Landsat 8 OLI	LULC and Shoreline Change Analysis	26-02-2004 27-01-2005 27-02-2022	30 m	USGS Earth Explorer
SRTM DEM	Slope, Relief	-	30m	USGS Earth Explorer
Geomorphology	Geomorphology	-	1:250k	bhukosh.gsi.gov.in
Socioeconomic data	Population, Tourism, Gross State Domestic Product (GSDP)	1991-2021 2001-2020	-	(censusindia.gov.in) (Directorate of economics and statistics) (Rbi.org.in)

**Deleted:** Month

**Deleted:** March

**Deleted:** and

**Deleted:** January

**Deleted:** March

221

222 **3.2 Tsunami Run-ups and Inundation**

223 Several attempts have been made to model tsunamis, to calculate inundation and  
 224 determine run-up heights, to evaluate their impact and hazards along mainland Indian coastal  
 225 areas (Rani et al., 2011; Srivastava et al., 2021). However, despite experiencing historical  
 226 tsunamis during the 31 December, 1881-Car Nicobar, 26 June, 1941-North Andaman, and the  
 227 26 December, 2004-Sumatra earthquakes, the south Andaman region is yet to be explored for  
 228 scenario hazard assessment. We used the Tohoku University's Numerical Analysis Model for  
 229 Investigation of Near field tsunamis (TUNAMI-N2) to simulate the tsunami run-ups and  
 230 impact using finite-difference methods to solve shallow water wave equations, incorporating  
 231 bathymetry, earthquake source parameters, and fault geometry (Imamura and Imteaz, 1995;  
 232 Imamura, 1996). In deep-sea regions with longer wavelengths a coarse grid spacing to model  
 233 linear effects is sufficient to resolve the wave with minimal error. As the tsunami wave  
 234 propagates from deep to shallow waters, where the wavelength shortens and the amplitude

**Deleted:** The 2004 earthquake rupture zone is divided into five segments by Ioualalen (2007) to simulate all stages of the tsunami. The earthquake source mechanism involves the rupture process, and magnitude is essential for tsunami hazard assessment. There

**Deleted:** several attempts

**Deleted:** ,

**Deleted:** , and

**Deleted:** .

**Deleted:** .

**Deleted:** For the propagation and run-up models, we used GEBCO bathymetry data with 81 arc seconds and 3 arc seconds resolution. The 26th

**Deleted:** 2004 Sumatra earthquake ruptured about 1400km in length. Considering different slip distributions for the five segments (Table 2)

**Deleted:** code is used to compute the four grids A, B, C, & D. The exterior

**Deleted:** (A) in a very large domain as

**Deleted:** transoceanic and is interpolated into the B, C,

**Deleted:** D grids. After giving the required inputs

**Deleted:** program is compiled



264 increases, it follow a non-linear pattern of amplitude dispersion, energy dissipation, bottom  
 265 friction and require finer resolution grids with more node points to accurately capture the wave  
 266 dynamics and minimize errors. The grid spacing should follow the Courant-Friedrich-Lewy  
 267 conditions for checking the convergence of the numerical code to a certain asymptotic limit  
 268 using following relationship.

$$\Delta x/\Delta t = \sqrt{2gh_{max}}$$

270 Where  $\Delta t$  and  $\Delta x$  are temporal and spatial grid sizes,  $h_{max}$  maximum still water depth in  
 271 the computational domain, and  $g$  is the gravitational acceleration. Based on above conditions  
 272 we used GEBCO bathymetry and topography data formatted into four grid of 81, 27, 9 and  
 273 3arc seconds resolutions at spacing ratio of 1:3 for grids A, B, C, and D, respectively.

274 The TUNAMI-N2 code uses Mansinha and Smylie's (1971) deformation model to  
 275 estimate the seafloor upliftment near the source and the focal mechanism solutions and fault  
 276 parameters are necessary to compute the initial deformation at the source at  $t=0$  seconds. In  
 277 addition to the grid resolution, the calibration requires earthquake source parameters (e.g., slip  
 278 distribution, fault length, and width), which we adopted based on Ioualalen (2007), Rani et al.  
 279 (2011), Mishra et al. (2014), and Srivastava et al. (2021) (Table 2). The five segments with  
 280 different slip distributions of Sumatra earthquake (December 26, 2004) with ~1400 km rupture  
 281 length (Ioualalen, 2007) are considered for modeling. We run the TUNAMI-N2 code with  
 282 above input parameters to get the directivity map, wave amplitudes (run-up heights) at different  
 283 tide-gauge locations, in the study region.

284 **Table 2** Tsunamigenic earthquake deformation parameters used to simulate different scenarios  
 285 a) 1881-Car Nicobar, and b) 1941-North Andaman earthquakes (Mishra et al., 2014), and  
 286 c) 2004-Sumatra (Ioualalen, 2007).

	<u>1881-Car Nicobar</u>	<u>1941 -North Andaman</u>	<u>2004 Sumatra Earthquake</u>				
Input Parameters			Seg1	Seg2	Seg3	Seg 4	Seg5
Longitude (DD)	<u>92.43</u>	<u>92.5</u>	94.57	93.90	93.21	92.60	92.87

Deleted: executed

Deleted: , and run-up heights.

Deleted: Earthquake source

Deleted: compute the deformation at the source along the

Deleted: Subduction Zone

Inserted Cells

Inserted Cells

Latitude (DD)	<u>8.52</u>	<u>12.1</u>	3.83	5.22	7.41	9.70	11.70
Focal Depth (km)	<u>15</u>	<u>30</u>	25	25	25	25	25
Strike angle (°)	<u>350</u>	<u>20</u>	323	348	338	356	10
Rake (°)	90	90	90	90	90	<u>90</u>	<u>90</u>
Slip (m)	<u>5</u>	<u>5</u>	18	23	12	12	12
Fault Length (km)	<u>200</u>	<u>200</u>	220	150	390	150	350
Fault Width (km)	<u>80</u>	<u>80</u>	130	130	125	95	95
Dip (°)	<u>25</u>	<u>20</u>	12	12	12	12	12
<b>Magnitude (Mw)</b>	<u>7.9</u>	<u>7.7</u>	<u>9.3</u>				

Inserted Cells

Inserted Cells

Inserted Cells

Inserted Cells

292

### 293 3.3 Shoreline Analysis in DSAS

294 The USGS's digital shoreline analysis system (DSAS) version 5.1 (an ArcGIS  
 295 extension) estimates shoreline changes. The procedures are executed in 4 steps: shoreline  
 296 digitization, baseline generation, transect generation, and computation of the shoreline change  
 297 rate (Raj et al., 2020; Natarajan et al., 2021). The digitized shorelines for 2004, 2005, and 2022  
 298 years have been added to a personal geodatabase in a single shapefile. The shoreline image  
 299 data is added to the attributes as MM/DD/YYYY, and the baseline is in the meter UTM  
 300 projected coordinate system. To estimate rates of change, DSAS uses baseline measurements  
 301 of a time series of shorelines and a shapefile (Leatherman, 2003). Generating transects involves  
 302 initially choosing a predefined set of parameters from the personal geodatabase, including  
 303 settings for the baseline and shoreline. Subsequently, we placed these transects perpendicular  
 304 to the shoreline, extending 800 m at intervals of 150 m along the entire shoreline, originating  
 305 from the baseline. A 50, m smoothing distance was applied using the 'cast transects' tool within  
 306 DSAS, to ensure a smoother outcome.

Deleted: To estimate shoreline changes, the

Deleted: of ArcGIS) is used

Deleted: rate of

Deleted: (Nithu

Deleted: .

Deleted: 2005and

Deleted: are

Deleted: and Clow, 1983). The process of generating

Deleted: meters

Deleted: meters

Deleted: To ensure a smoother outcome, a

Deleted: -meter

Deleted: . In this study, we employ statistical methodologies such as the End Point Rate (EPR) and Net Shoreline Movement (NSM)

Deleted: analyze the data.

307 The evaluation of uncertainty encompasses natural and anthropogenic forces such as  
 308 wind, waves, tides, currents, and human influences, along with the accuracy of measurement  
 309 techniques, including digitization, interpretation, and GPS error. The uncertainty in the

326 shoreline analysis is due to the influence of tides on the Landsat satellite imagery, which is  
 327 minuscule in the extensive coastline of the study area. The tide gauge data of Port Blair station  
 328 for 2004-2005 and 2022 are unavailable in the Permanent Service for Mean Sea Level  
 329 (PSMSL) database (<https://psmsl.org/data/obtaining/stations/206.php>). We calculated  
 330 uncertainty of 7.46m and 7.13m for 2018-2019 and 2019-2020, respectively, and the same is  
 331 adopted for 2022 owing to similar ranges. To quantify uncertainty, we have adopted a  
 332 confidence interval of 90% and assigned a shoreline uncertainty value of 10 meters as per the  
 333 recommendations of the United States Geological Survey (USGS) under the National  
 334 Assessment of Shoreline Change project (Himmelstoss et al., 2021; Den and Oele, 2018 and  
 335 Joetidawati, 2016). We used End Point Rate (EPR) and Net Shoreline Movement (NSM)  
 336 methods to analyze the shoreline change. The statistical mean of these parameters was  
 337 computed using USGS's DSAS tool (Himmelstoss et al., 2021).

338 **3.3.1 Net Shoreline Movement (NSM)**

339 NSM is a statistical parameter used to determine the net change in the shoreline position over  
 340 a specific period by finding the perpendicular distance between the most recent shoreline (in  
 341 this case, 2022) and the oldest shoreline (2004) along each transect. The formula for NSM can  
 342 be expressed as:

$$NSM = \{ d_{2022} - d_{2004} \} m$$

344 **3.3.2 End Point Rate (EPR)**

345 EPR is a statistical parameter quantifying the shoreline change rate over time, is calculated by  
 346 dividing the Net Shoreline Movement (NSM) by the time elapsed between the oldest and most  
 347 recent shoreline measurements, which indicates the rate of erosion or accretion. It is important  
 348 to have data from at least two shoreline dates (Dolan et al., 1991; Crowell et al., 1997). The  
 349 formula for EPR can be expressed as follows:

$$EPR = \left\{ \frac{d_{2022} - d_{2004}}{t_{2022} - t_{2004}} \right\}$$

**Deleted:** . It is calculated

**Deleted:** actual

**Deleted:** placed perpendicular to the shorelines.

**Deleted:** used to quantify

**Deleted:** rate of

**Deleted:** . It

**Deleted:** . The formula for EPR can be expressed as This calculation provides a measure of how much the shoreline has shifted per year, indicating

**Deleted:** .

**Deleted:** .

362 **3.4 Land Use Land Cover Analysis (LULC)**

363 The LULC map uses Landsat 5 TM (2004 and 2005) and Landsat 8 OLI (2022). False Colour  
364 Composite (FCC) satellite images combine near-infrared, red, and green bands to delineate five  
365 classes: Forest, built-up, Cropland, Water bodies, and Inundated areas. (Prabhbir and Kamlesh,  
366 2011). Tone, texture, size, shape, pattern, association, and other visual interpretation techniques  
367 also were used to interpret different land use classes. Maximum likelihood is a supervised  
368 classification method used in this study to detect LULC change. Each pixel in the classified  
369 Landsat images varies over time due to changes in land cover.

370 **4. Results**

371 An analysis of the 2004 tsunamigenic earthquake's impact on the South Andaman  
372 region, focusing on tsunami directivity, arrival times, run-up heights, shoreline changes, and  
373 LULC impact, is examined in detail.

374 **4.1 Tsunami studies along the South Andaman Region**

375 We have considered three tsunamigenic seismic scenarios, namely, a) the 1881-Car  
376 Nicobar earthquake, b) the 1941-North Andaman earthquake, and c) the 2004 Sumatra  
377 earthquake, and generated the directivity and run-up model (Fig. 3). The directivity map shows  
378 that most of the energy propagation is in the East-West direction (Fig. 3 a,b,c), and the  
379 shallower waters surrounding the Andaman and Nicobar Islands has significance influence on  
380 the east-west propagation of tsunamis (Singh et al., 2012). The run-up height along the eastern  
381 coast of South Andaman is greater than the western coast (Fig. 3 b', c', d'; Table 3). This  
382 difference is due to the wider continental shelf on the Western coast of the south Andaman  
383 region and shallow water depths. In the case of a higher magnitude of tsunamigenic earthquakes  
384 in the Car Nicobar or the North Andaman region, higher run-ups will be observed along the  
385 gauge locations, which are considered for the present study (Table 3).

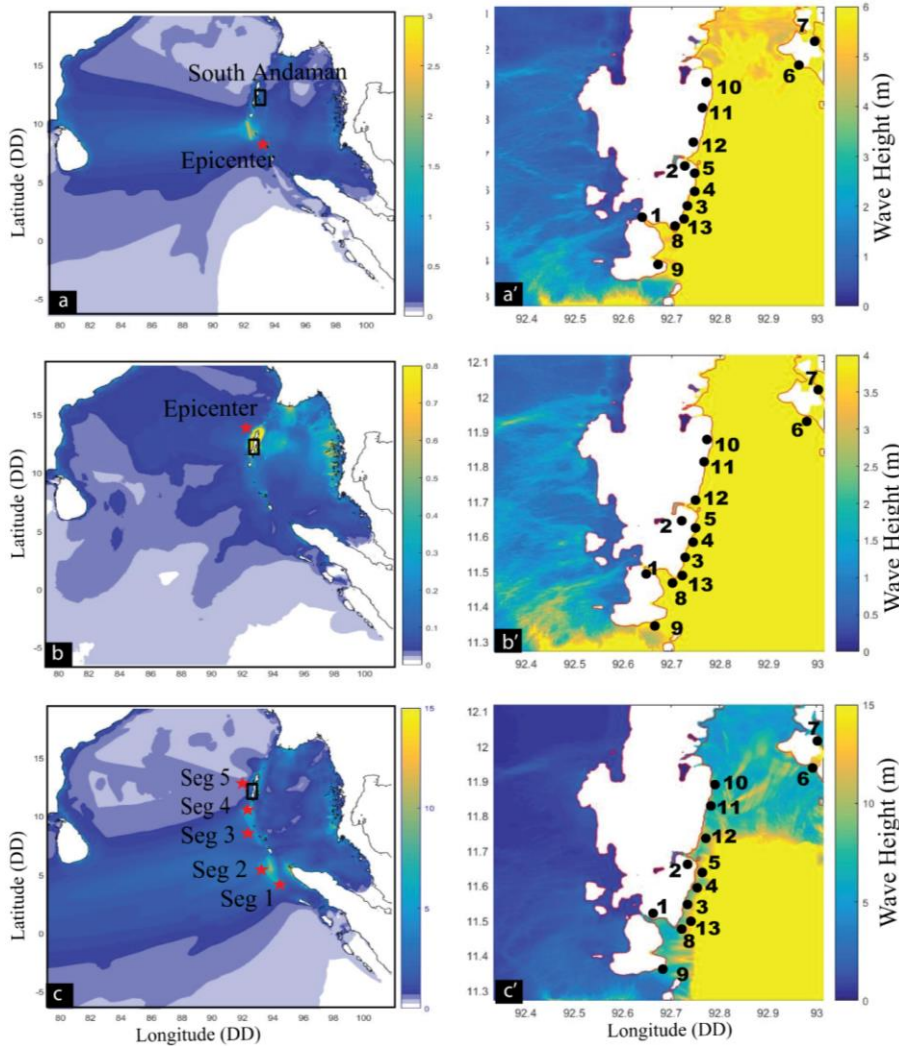
Deleted: different

Deleted: area

Deleted: The 2004 tsunamigenic earthquake is modeled to quantify the tsunami propagation, arrival times, and run-ups at different locations along the South Andaman region. The initial deformation at the source is computed for the fault parameters (Table 2). The Directivity map shows that most of the energy propagation is in the East-West Direction (Fig. 3).

394 The arrival times of tsunamis vary from 21.75 minutes to 58 minutes across locations  
395 for these earthquakes, with the 1881-Car Nicobar earthquake generally resulting in the shortest  
396 arrival time (Fig. 3; Table 3). The run-up heights range from 1-13 m at different locations (Fig.  
397 3; Table 3), which were influenced by earthquake magnitude, the source's proximity to  
398 observation locations, and the local coastal topography that also affected inundations. The  
399 extent of inundation, representing the area covered by the tsunami, ranges from 10m to 950m,  
400 with a wide variation across locations and earthquake events. The 2004 Andaman Sumatra  
401 earthquake resulted in higher run-up heights and inundations compared to the 1881 Car  
402 Nicobar, and 1941 Andaman earthquakes and caused extensive damage. Therefore, we  
403 considered the 2004- Andaman Sumatra earthquake for a detailed analysis of hazard  
404 assessment and scenario analysis. The arrival times (Minutes), run-up height (meter), and  
405 Inundation extent (meter) at 13 different locations along the South Andaman region by the  
406 2004 Sumatra earthquake (Table 3) are considered for further analysis.

Deleted: is



408  
409 *Figure 3: (a) Directivity and (a') wave run-up height for the 1881-Car Nicobar, (b and b') for the 1941-Andaman,*  
410 *and (c and c') for the 2004-Sumatra earthquakes.*

411  
412 **Table 3** *Estimated Arrival times, Run-up heights, and inundations at the studied locations from*  
413 *sunamigenic a) 1881-Car Nicobar, b)1941-North Andaman earthquakes, and c) 2004-Sumatra*  
414 *earthquake sources. The SN of locations is common for Figs. 3 and 4.*

<u>SN</u>	<u>Gauge Locations</u>	<u>Longitude Latitude (DD)</u>	<u>Earthquake Sources</u>	<u>Arrival Time(Min.)</u>	<u>Run-up (m)</u>	<u>Inundation (m)</u>
1	Wandoorjetty	92.614750, 11.581667	a) 1941-North Andaman	22.5	1.25	180
			b) 1881 Car Nicobar	32.80	2.21	200
			c) 2004 - Sumatra	36.5	3.5	450

Moved (insertion) [2]



2	Bombooflat	92.715417, 11.700722	a) 1941-North Andaman	24.55	2.23	350
			b) 1881 Car Nicobar	31.2	2.35	650
			c) 2004 - Sumatra	42	5.5	90
3	Corbyns Cove Beach	92.770916, 11.642372	a) 1941-North Andaman	22.3	2.1	320
			b) 1881 Car Nicobar	28.8	2.3	580
			c) 2004 - Sumatra	33	12.7	900
4	South Point, Port Blair	92.702917, 11.652389	a) 1941-North Andaman	22	2.12	280
			b) 1881 Car Nicobar	28.4	2.31	500
			c) 2004 - Sumatra	31.5	9.6	550
5	Thirupatti Temple	92.703861, 11.581694	a) 1941-North Andaman	21.75	1.42	360
			b) 1881 Car Nicobar	46.5	1.65	400
			c) 2004 - Sumatra	38	1	200
6	Radha Nagar	92.951722, 11.979306	a) 1941-North Andaman	52	2.1	180
			b) 1881 Car Nicobar	54	3.8	220
			c) 2004 - Sumatra	54	2.6	156
7	Govinda Nagar	92.989139, 12.030167	a) 1941-North Andaman	56	1.8	220
			b) 1881 Car Nicobar	58	3.2	190
			c) 2004 - Sumatra	58	3.6	195
8	Chidiyatopu	92.716639, 11.499306	a) 1941-North Andaman	21.75	1.79	300
			b) 1881 Car Nicobar	26.5	2.05	500
			c) 2004 - Sumatra	36	3.9	585
9	Rutland Island	92.703818, 11.431497	a) 1941-North Andaman	25.9	1.01	585
			b) 1881 Car Nicobar	26.55	1.44	380
			c) 2004 - Sumatra	27	6	700
10	Shoal Bay	92.795963, 11.934202	a) 1941-North Andaman	34.8	1.77	180
			b) 1881 Car Nicobar	42.5	1.45	220
			c) 2004 - Sumatra	56	13	950
11	Potatang	92.801282, 12.027380	a) 1941-North Andaman	36	1.5	200
			b) 1881 Car Nicobar	46	1.4	180
			c) 2004 - Sumatra	58	12.5	210
12	Madhuban Bay	92.785534, 11.782775	a) 1941-North Andaman	32	1.9	180
			b) 1881 Car Nicobar	40	1.5	200
			c) 2004 - Sumatra	54	6.9	210
13	Brichgunj	92.770162, 11.618980	a) 1941-North Andaman	28	1.3	200
			b) 1881 Car Nicobar	32	4	300
			c) 2004 - Sumatra	30	10	585

415 The results show that the run-up heights range from 1 to 13 m, arrival times range from  
416 27 to 58 min, and the inundation extent range from 90 to 950m, suggesting a significant  
417 variability in the tsunami's impact across the South Andaman Region. Due to the effects of the  
418 2004 tsunami, the stagnation of tsunami water in the agricultural lands and low-lying areas of  
419 the Wandoor region resulted in increased soil salinity (Fig. 4a); it also damaged the bridge in

Deleted: 950 m. This suggests

Deleted: of the tsunami

422 the Bombooflat area (Fig. 4b), and houses near the Sippighat area (Fig. 4c, d). Shoal Bay  
 423 recorded the highest inundation extent of 950m and experienced the highest run-up height of  
 424 13m, indicating significant wave impact (Fig. 3b; Table 3). Corbyn's Cove Beach and Rutland  
 425 Island experienced significant inundation distances, exceeding 700m (Fig.3b, Table 3).  
 426 Potatang, Corbyns Cove Beach, and Brichgunj also recorded relatively high run-up heights that  
 427 exceeded 9m (Table 3). Most locations experienced arrival times between 27 and 58 minutes,  
 428 indicating a relatively quick propagation of the tsunami wave. Jain et al. (2005) mentioned that  
 429 tsunami waves arrived between 40 and 50 minutes in the Andaman and Nicobar Islands. Our  
 430 results agree with the tsunami run-up heights estimation by Cho et al. (2008) and Perna et al.  
 431 (2015) at a few locations in the present study. South Andaman experienced significant  
 432 inundations during the 2004 Sumatra earthquake, highlighting the urgent need for robust  
 433 mitigation and preparedness measures in these vulnerable coastal regions. We aim to contribute  
 434 to this broader goal by providing essential data and insights to support evidence-based decision-  
 435 making and mitigate the adverse impacts of tsunamis on coastal populations. The study will  
 436 provide workable input to the local risk management strategies involving local communities,  
 437 optimizing evacuation planning, enhancing early warning systems, fortifying infrastructure  
 438 resilience, and adopting a multi-hazard risk assessment approach (National Research  
 439 Council, 2011).

**Deleted:** 950 meters

**Deleted:** 13 meters

**Deleted:** Corbyns

**Deleted:** ,

**Deleted:** 700 meters

**Deleted:** 9 meters (Table 3). The tsunami arrived at Thirupatti Temple after 38 minutes, suggesting a delayed impact compared to other locations.

**Deleted:** At some locations, however, the tsunami arrived early.

**Deleted:** have

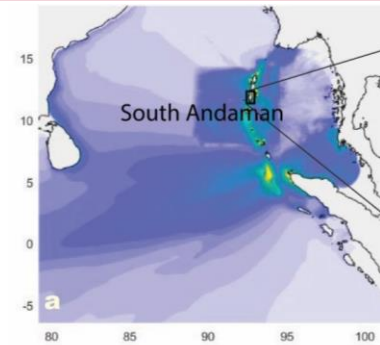
**Deleted:** to

**Deleted:** also

**Deleted:** who computed the tsunami runup heights

**Deleted:** of the

**Deleted:** considered



**Deleted:**



Figure 4: (a) Stagnation of Tsunami water in the agricultural field and Low-laying areas in Port Blair, (b) damaged bridge in Bombooflat, (c, d) damaged house in the Sippighat area near Port Blair (Photo: 01/03/2023). The number on the field photograph corresponds to respective locations as in Fig. 3.

#### 4.2 Shoreline Change during Tsunami (2004-2005) and post-tsunami (2005-2021)

The south Andaman coasts are divided into seven zones based on proximity with the inundation studies to calculate NSM and EPR to understand the short-term and long-term changes impact of coastal erosion (Fig. 5, Supplement Fig. S1-S7). The NSM and EPR are calculated over two separate time frames to comprehend the damages caused by tsunamigenic and regular wind-wave-surge events in South Andaman Island. These zones were used to understand erosion and accretion rates between (i) 2004 - 2005 (Fig. 5a) and (ii) 2005-2022 (Fig. 5b). The EPR and NSM values from 2004 to 2005 indicate the direct effect of tsunami waves, whereas 2005 to 2022 values represent periodic wind-wave-surge dynamics. Periodic coastal shoreline changes refer to the regular and repeating fluctuations in the position of the shoreline along the coast. Natural and human-induced factors can influence these changes. A total of 1,083 transects are created at 50-m intervals, distributed among the zones as follows:

- Deleted: 3
- Deleted: Directivity of the tsunami Wave Propagation of December 2004 Sumatra tsunami (b) Run-ups at different locations along the south Andaman Coast (c) showing
- Deleted: land
- Deleted: Area
- Deleted: d) Fully
- Deleted: construction
- Deleted: .
- Deleted: shows damage to the
- Deleted: near
- Moved up [2]: ¶ Table 3 Estimated
- Deleted: Run-up heights, Arrival Times, and inundations at the study region from the Sumatra tsunami ¶ SN
- Deleted: Net shoreline movement (
- Deleted: ),
- Deleted: End Point Rate (
- Deleted: )
- Deleted: 4
- Deleted: rates
- Deleted: 4a),
- Deleted: 4b
- Deleted: These changes can be influenced by natural
- Deleted: .
- Deleted: meter

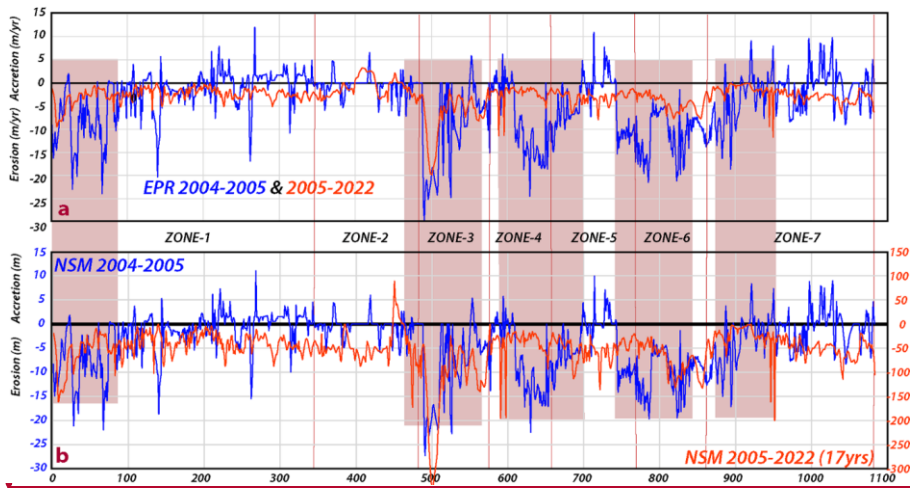
503 Zone 1 (339 transects), Zone 2 (147 transects), Zone 3 (89 transects), Zone 4 (74 transects),  
 504 Zone 5 (137 transects), Zone 6 (73 transects), and Zone 7 (220 transects). The shoreline  
 505 variation rates indicate positive accretion and negative erosion (Fig. 6, Table 4). The EPR  
 506 Changes in meters per year (m/y) for the periods 2004-2005 show a higher erosion rate  
 507 compared to 2005-2022, particularly in Zones 3, 4, and 5 (Fig. 6a). The NSM, focused on two  
 508 distinct time frames, indicate the NSM rates during the tsunami, for the year of 2004-2005, and  
 509 the NSM rates over the extended 17-year period from 2005 to 2022 are measured in meters  
 510 (Fig. 6b). The detailed analysis of the maximum (accretion), minimum (erosion), and mean  
 511 shoreline changes for each of the seven zones that occurred during the tsunami event and the  
 512 post-tsunami period are discussed below.

Deleted: both  
 Deleted: 5  
 Deleted: rate  
 Deleted: 5a  
 Deleted: rates,  
 Deleted: (Fig. 5b),  
 Deleted: 5c

513  
 514 *Figure 5: Shoreline changes observed (a) during 2004-05 due to the tsunamigenic process and (b) from 2005-*  
 515 *2022 due to wind wave surges overlaid on Google Earth images (@Google Earth). The affected coastline is*  
 516 *subdivided into seven distinct zones for detailed analysis.*

Deleted: 4



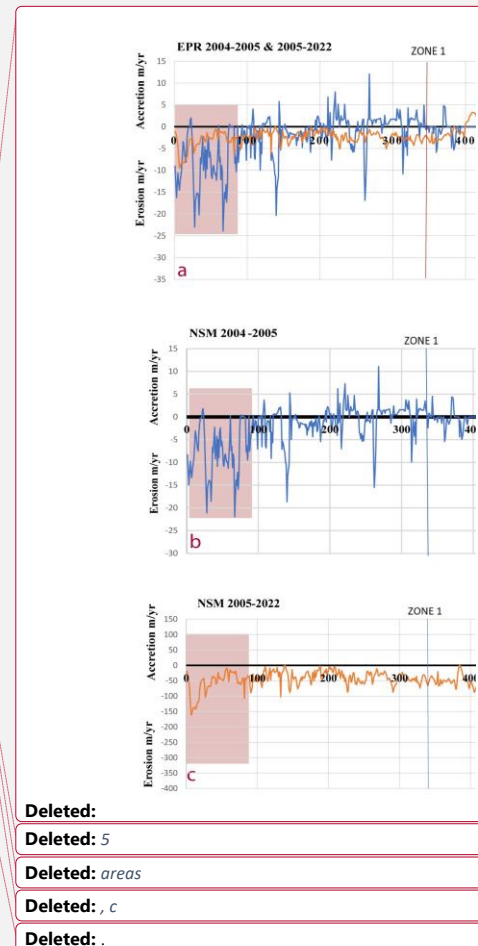


525  
526 Figure 6: (a) The rates of erosion and accretion in seven distinct Zones along the South Andaman shoreline using  
527 EPR methods, and (b) NSM have been conducted between the years 2004-2005 and 2005-2022. Highlighted color  
528 indicating high erosion zone

529  
530 **Table 4** Shoreline change in southern Andaman is observed for 2004-2005 and 2005-2022  
531 using USGS's DSAS methods (Himmelstoss et al., 2021).

ZONE		2004-2005		2005-2022	
		EPR(m/y)	NSM(m)	EPR(m/y)	NSM (m)
ZONE 1	Mean	-2.85	-2.62	-2.55	-43.57
	Minimum	-23.9	-21.29	-9.44	-161.21
	Maximum	12.05	11.06	0	0
ZONE 2	Mean	-0.54	-0.50	-1.0639	-18.174
	Minimum	-7.17	-6.58	-4.56	-77.93
	Maximum	6.54	6	3.25	55.56
ZONE 3	Mean	-9.92	-8.11	-7.10	-121.51
	Minimum	-24.71	-23.27	-19.87	-339.51
	Maximum	5.58	4.37	-1.02	-17.42
ZONE 4	Mean	-7.92	-7.72	-2.24	-38.34
	Minimum	-24.47	-22.46	-11.42	-195.03
	Maximum	6.23	5.72	-0.79	-13.42
ZONE 5	Mean	-6.594	-6.05	-2.94	-50.26
	Minimum	-21.47	-19.7	-7.95	-135.83
	Maximum	10.88	9.99	-1.03	-17.54
ZONE 6	Mean	-9.74	-8.94	-4.92	-84.05
	Minimum	-21.18	-19.44	-7.75	-132.39
	Maximum	-1.46	-1.34	-1.86	-31.73
ZONE 7	Mean	-2.16	-1.986	-2.43	-41.56
	Minimum	-18.65	-17.29	-11.7	-199.96
	Maximum	9.77	8.97	-0.04	-0.61

532



Deleted:

Deleted: 5

Deleted: areas

Deleted: , c

Deleted: .

538 ZONE 1: This zone experienced a combination of erosion and accretion between 2004-05 and  
539 2005-21. The maximum erosion rates are observed at Megapoda, with an EPR of -23.9  
540 m/y. and -9.44 m/y., NSM analysis shows the estimated erosion is -21.29m and -161.21m  
541 respectively (Fig. [S1](#) a, b, Table [4](#)). The southern part of South Andaman Island has more  
542 shoreline erosion rather than accretion, which can be attributed to the heightened impact  
543 of tsunamis on the southern region, a phenomenon that is more significant when  
544 compared to the northern part of South Andaman Island. These Sediments eroded from  
545 one coastline area are often transported along the shoreline by the longshore currents.  
546 The angle of wave approach creates these currents and is responsible for moving  
547 sediment parallel to the coastline.

Deleted: SM 1

Deleted: 6

548 ZONE 2: This zone experienced a combination of erosion and accretion between 2004-05 and  
549 2005-21. The maximum rate of erosion is -7.17 m/y and -4.56 m/y (EPR) was recorded  
550 at IOC Colony, while the maximum accretion rate of 6.54 m/y and 3.25 m/y (EPR) was  
551 observed at Ashwin Nagar Respectively. The NSM analysis indicated a shoreline retreat  
552 of -6.58 m at IOC Colony and -77.93 m advancement at Ashwin Nagar. The jetties in the  
553 Jungli Ghat port played a role in controlling erosion and accretion at these sites (Fig. [S2](#),  
554 Table [4](#)).

Deleted: SM-2

Deleted: 6

555 ZONE 3: This zone experienced a combination of erosion and accretion between 2004-05 and  
556 2005-21. The maximum erosion rate is -24.71 m/y and -19.87 (EPR) at Flat Bay, while  
557 the maximum accretion rate is 5.58 m/y and (EPR) at NLC Limited. The NSM analysis  
558 revealed a shoreline retreat of -23.27 m and -339.51 m at Flat Bey. High wave energy  
559 and exposure to strong currents, which are more common near Flat Bay, can lead to  
560 increased erosion of mangrove shorelines (Fig. [S3](#), Table [4](#)).

Deleted: SM 3

Deleted: 6

561 ZONE 4: This zone experienced a combination of erosion and accretion between 2004-05 and  
562 2005-21. The maximum erosion rate is -24.47 m/y at Ferrargunj and -11.24 m/y (EPR)



569 at PLK Creek Resort, NSM estimated erosion is -22.46 m and -195.03m at Chouldari  
 570 (Fig. S4). We observed the shoreline erosion area using the Landsat time-lapse satellite  
 571 images between 2004-2005, and 2022 near Flat Bay, South Andaman, has revealed  
 572 noteworthy environmental changes. The dark blue color observed in 2004 and 2005  
 573 indicates the presence of deep-water bodies, whereas the light blue color in the 2022  
 574 image suggests the water bodies have become shallow with significant fresh sediment  
 575 load (Fig. 7; Table 4).

Deleted: SM 4

Deleted: .



577  
 578 Figure 7 shows a time-lapse satellite imagery of Landsat 8 FCC near the Flat Bay area (marked in yellow circle)  
 579 during the years 2004 and 2005 showing robust mangrove coverage is evident. However, when comparing the  
 580 Landsat 8 image in 2022 and the corresponding Google Earth image (@Google Earth), it is apparent that the  
 581 mangrove ecosystem in this area has experienced substantial erosion and the development of Solar panels.  
 582

Deleted: 6

583 ZONE 5: The maximum erosion rate of -21.47 m/y (2004-05) and -7.95 (EPR 2005-22) is  
 584 recorded at Mithakhari. According to the NSM analysis, the shoreline retreated by -19.7  
 585 m and -132.39m at Mithakhari (Fig. S5). In this zone, Coastal development,

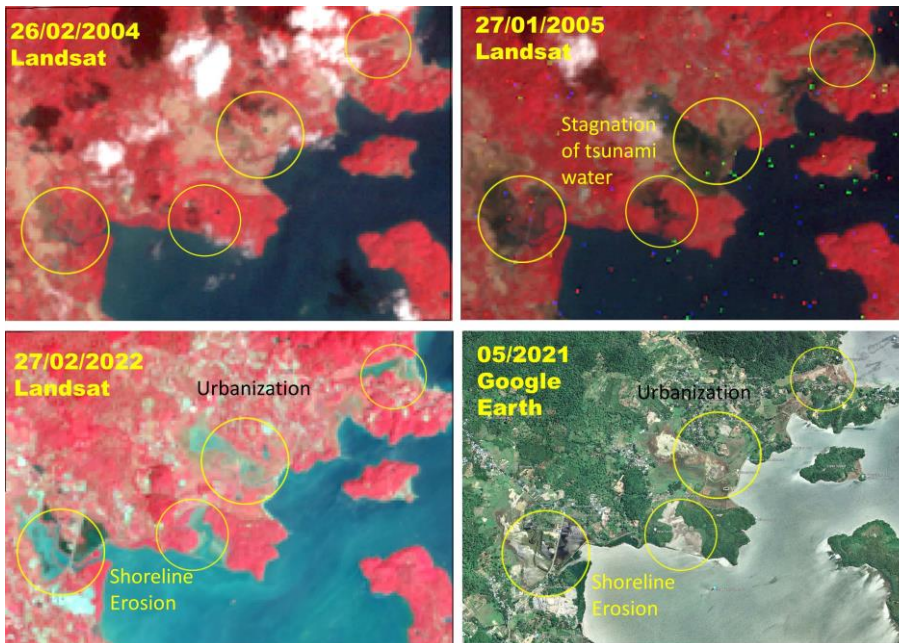
Deleted: 39 meters

Deleted: SM 5

591 infrastructure construction, and alteration of natural hydrological patterns can disrupt  
592 sediment transport and exacerbate erosion (Fig. 8; Table 4).

Deleted: .

593



594

595 *Figure 8 shows Landsat 8 time-lapse imagery and @ Google Earth imagery near the Ograbraj and Mithakhari*  
596 *region depicting the erosion activity during and after the tsunami and the imagery shows a significant growth in*  
597 *the built-up areas surrounding the tsunami-affected areas in 2004.*

Deleted: 7

598

599 ZONE 6: This zone is predominantly affected by erosion, with no observed accretion. The  
600 maximum erosion rate is -21.18 m/y and -7.75 m/y (EPR) at Namunaghar, and the NSM  
601 estimated erosion is -19.44 m and -132.39m at Namunaghar (Fig. S6). In February 2004,  
602 immediately before the catastrophic tsunami event, there was no observable presence of  
603 stagnant water in the area (Fig. 9). However, by January 2005, following the tsunami, the  
604 images distinctly exhibited the stagnant water. In February 2022, the same location  
605 exhibited substantial shoreline erosion within the extensive mangrove and agricultural  
606 area, accompanied by increased urban development along the shoreline. The progression

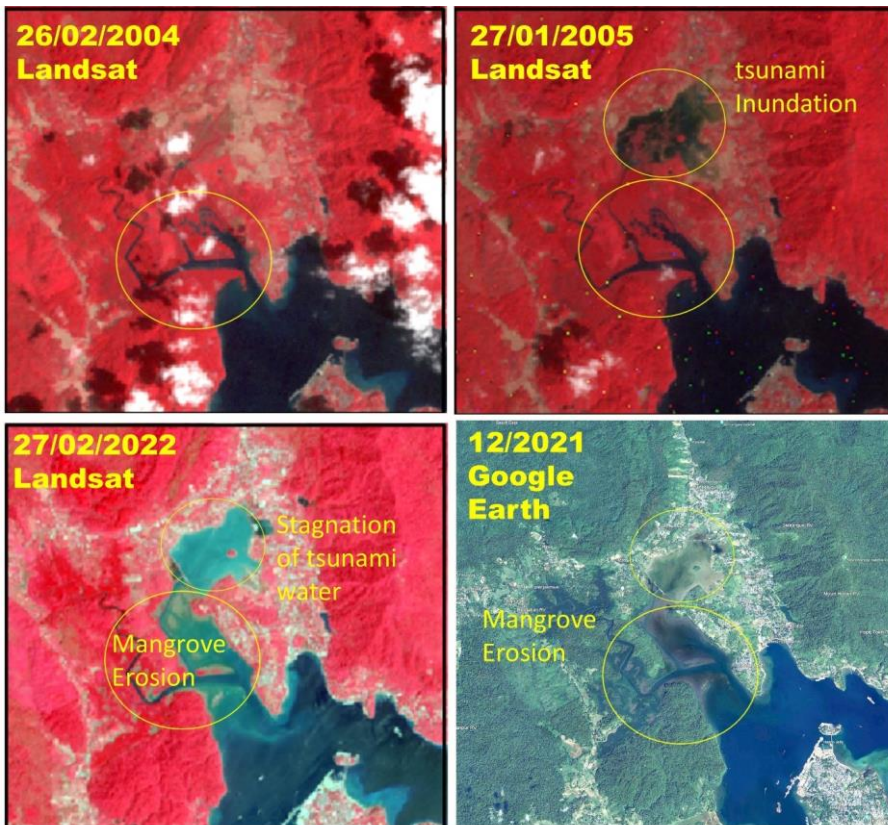
Deleted: SM 6

Deleted: 8

611 of urban development was also validated using Google satellite imagery. The sediment  
612 carried by ocean currents deposited in low-lying areas revealed caused shallowing and  
613 significant changes in ocean water color.

Deleted: progression is

614



615

616 Figure 9 shows the Change detection of the shoreline using Landsat 8 time-lapse imagery and © Google Earth  
617 imagery for 2004 before, 2005 after the tsunami, and the 2022 present status of the shoreline.

Deleted: 8

618

619 ZONE 7: This zone experienced a combination of erosion and accretion between 2004-05 and  
620 2005-21. The maximum erosion rate is -8.36 m/y and -11.7 m/y (EPR) at Shore Point,  
621 while the maximum accretion rate is 9.77 m/y (EPR). The NSM analysis indicated an

624 erosion of -17.29 m at Shore Point and -199.96 m at North Bay (Fig. S7; Table 4).

Deleted: meters

625 Notably, a tsunami with a height of 9.6 m is observed at Shore Point.

Deleted: SM 7

Deleted: meters

626 The natural rate of shoreline movement in the South Andaman region has increased  
627 following the tsunami event, which is attributed to several factors, including the removal of  
628 vegetation cover, the softening of exposed bedrock, and the destabilization of unconsolidated  
629 materials caused by the tsunami, all of which have made the region more susceptible to erosion  
630 (Yunus et al., 2016). Comparing the erosion and accretion rates suggests the erosion rates were  
631 significantly less during the 2005-2022 period in comparison to the 2004-05 tsunami,  
632 highlighting the adverse effect of the tsunami.

Deleted: between the 2004-05 and 2005 -2022 periods, it is observed that

Deleted: in the latter years

### 633 4.3 Land Use and Land Cover (LULC) Analysis

634 The LULC is categorized into 5 distinct classes: Built-up, Forest, Inundation, Cropland,  
635 and water Bodies (Fig. 10). The overall accuracy obtained is 90.11%, 89.96%, and 90.30%  
636 with a quantitative assessment of  $K_{hat}$  (Kappa) coefficient is 0.78, 0.762 and 0.79 for 2004,2005  
637 and 2022 images, respectively, (Table S1). Our primary objective is to determine the extent of  
638 land use pattern changes from 2004 to 2022 in areas affected by the 2004 tsunami. Several  
639 researchers have already examined the vulnerability and impact of the 2004 tsunami on South  
640 Andaman, including (Velmurugan et al., 2006; Debjani et al., 2012; Sachithanandam,2014).

Deleted: 9

Deleted: 80%, 83

Deleted: 82

Deleted: 741

Deleted: 759

Deleted: .

Deleted: .

Deleted: .

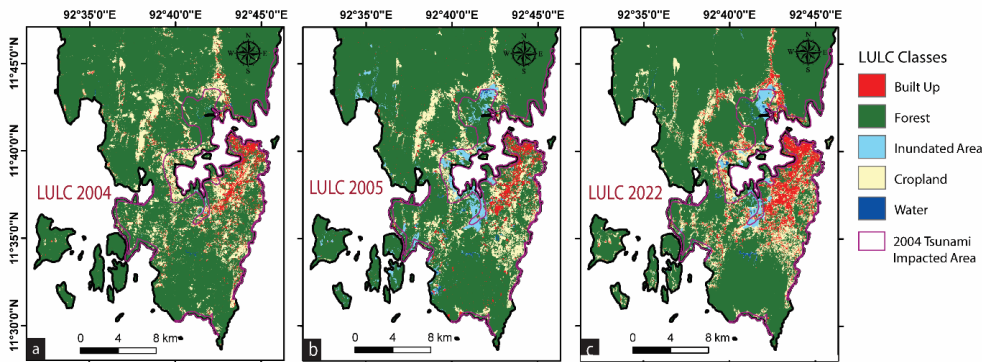
641 The LULC classification for the South Andaman region in tsunami-impacted areas in  
642 the years 2004, 2005, and 2022 reveals significant changes (Fig. 10, Table 5). 1) The built-up  
643 area decreased from ~7.38% in 2004 to 6.23% in 2005, marking a 1.15% decrease. However,  
644 it subsequently increased by 11.11% by 2022. 2) Cropland coverage decreased from around  
645 22.12% in 2004 to ~11.93% in 2005, indicating a substantial reduction of 10.19%. It then  
646 increased to 17.15% by 2022. 3) Inundation areas increased from about 3.29% in 2004 to  
647 27.65% in 2005, showing a notable rise of 24.36%. However, by 2022, they decreased by  
648 ~18.57%. 4) Forested areas saw a significant decrease from ~66.46% in 2004 to about 51.10%

Deleted: 9

Deleted: ):



665 in 2005, signifying a reduction of 15.36%. This decrease persisted in 2022, remaining at  
 666 ~51.10%. 5) Water bodies covered around 0.62% of the area in 2004, which increased slightly  
 667 to about 0.76% in 2005. By 2022, there is a more significant increase, reaching 2.05%.



668  
 669 *Figure 10 (a) LULC 2004 (b) LULC 2005, and (c) LULC 2022 in tsunami-impacted areas (pink color) and South*  
 670 *Andaman.*

671 **Table 5** LULC Analysis for 2004, 2005 to 2022 in tsunami impacted area

LULC	2004 Area in km <sup>2</sup>	2004 % of Area	2005 Area in km <sup>2</sup>	2005 % of Area	2022 Area in km <sup>2</sup>	2022 % of area
Built-Up	3.57	7.38	3.01	6.23	5.38	11.11
Forest	32.19	66.46	25.79	53.40	24.74	51.10
Inundation Area	1.64	3.39	13.36	27.65	8.99	18.57
Cropland	10.71	22.12	5.76	11.93	24.74	17.15
Water Bodies	0.30	0.62	0.36	0.76	0.99	2.05
Total Area (Sq. Km)	48	100	48	100	48	100

672  
 673 The LULC classification for the South Andaman region in the years 2004, 2005, and 2022  
 674 shows significant changes (Figure 10, Table 6)

675 **1) Built-Up Area:** In 2004, the built-up area covered 19.92 km<sup>2</sup>, constituting ~3.84% of the  
 676 total study area. By 2005, this area had reduced to 17.66 km<sup>2</sup>, accounting for 3.41% of

Deleted: 9

Deleted: Area

Deleted: 9

680 the total area. by 2022, there was a significant expansion, with the built-up area  
 681 occupying 45.07 km<sup>2</sup>, representing 8.68% of the total region.

682 **2) Forest:** In 2004, forests dominated the landscape, covering 432.85 km<sup>2</sup>, which was  
 683 approximately 83.43% of the total study area. By 2005, this forested area slightly  
 684 decreased to 420.79 km<sup>2</sup>, comprising 81.27% of the total area. However, by 2022, the  
 685 forest cover continued to decline, with an area of 408.66 km<sup>2</sup>, accounting for 78.78% of  
 686 the total region.

687 **3) Inundation Area:** In 2004, the inundation area was limited, covering 3.40 km<sup>2</sup> or 0.65% of  
 688 the total area. In 2005, there was a substantial increase, expanding to 28.41 km<sup>2</sup>, which  
 689 represented 5.48% of the total area. By 2022, the inundation area decreased to 13.89 km<sup>2</sup>,  
 690 making up 2.66% of the total region.

691 **4) Cropland:** Cropland covered 61.77 km<sup>2</sup> in 2004, accounting for 11.90% of the total study  
 692 area. By 2005, this area reduced to 49.34 km<sup>2</sup>, representing 9.53% of the total area. In  
 693 2022, the cropland area further decreased to 48.65 km<sup>2</sup>, making up 9.37% of the total  
 694 region.

695 **5) Water Bodies:** In 2004, water bodies covered a small area of 0.83 km<sup>2</sup>, approximately 0.16%  
 696 of the total area. By 2005, this area slightly increased to 1.54 km<sup>2</sup>, constituting 0.29% of  
 697 the total region. There was a more significant expansion during 2022, with water bodies  
 698 occupying 2.45 km<sup>2</sup>, accounting for 0.47% of the total area.

Deleted: which was

Deleted: In 2022, there

699 **Table 6** LULC Analysis for 2004, 2005 to 2022 in the Study region

LULC	2004 Area in km <sup>2</sup>	2004 % of Area	2005 Area in km <sup>2</sup>	2005 % of Area	2022 Area in km <sup>2</sup>	2022 % of <u>area</u>
Built-Up	19.92	3.84	17.66	3.41	45.07	8.68
Forest	432.85	83.43	420.79	81.27	408.66	78.78
Inundation Area	3.40	0.65	28.41	5.48	13.89	2.66
Cropland	61.77	11.90	49.34	9.53	48.65	9.37
Water Bodies	0.83	0.16	1.54	0.29	2.45	0.47

Deleted: Area



Total Area (Sq. Km)	518	100	518	100	518	100
---------------------	-----	-----	-----	-----	-----	-----

703

704 **5. Discussion**

705 The complex interaction between geomorphology, shoreline change, LULC changes, and  
 706 economic factors in tsunami vulnerability and impact assessment in South Andaman is  
 707 discussed below;

708 **5.1 Shoreline changes VS LULC**

709 The impact of tsunamis varies due to differences in landforms, relief, slope, elevation, and  
 710 the presence (or absence) of natural barriers such as coral reefs and mangroves. It has been  
 711 observed that for a given water depth on the shelf, if the continental slope is steeper, greater  
 712 mangrove cover, greater relief, and higher elevation can result in a greater amount of energy  
 713 being reflected, leading to a smaller tsunami wave height on the shelf. On the other hand, with  
 714 a flatter slope, low relief, and less vegetation cover area on the coastal side, the reduced  
 715 reflection and effect of shoaling can increase tsunami wave height (Siva et al., 2016). Coastal  
 716 erosion is a natural process in south Andaman that occurs when waves, currents, tsunamis, and  
 717 tides erode the shoreline, removing sediment and land over time. Factors such as sea-level rise,  
 718 wave energy, storm events, and human activities can contribute to increased rates of erosion.

719 Over time, the geomorphological landforms continue to shape and modify the landscape.  
 720 However, human activities and developmental pressures are significant drivers of LULC  
 721 change in South Andaman (Fig. 10 a, b, c). Common LULC changes observed in the area  
 722 include deforestation for urban expansion, conversion of land for agriculture, infrastructure  
 723 development, and alterations to the coastal zone (Yuvaraj et al., 2014; Thakur et al., 2017;  
 724 Jaman et al., 2022). The interaction between geomorphology and LULC change is particularly  
 725 evident in the coastal regions of South Andaman, where coastal erosion and accretion processes  
 726 influence both LULC patterns and development decisions. The erosion occurring near the

Deleted: back

Deleted: .

Deleted: 9

730 shoreline leads to the loss of valuable land, affecting agricultural areas and forest regions (Fig.  
731 7.8,9). Conversely, accretion processes can contribute to the growth of coastal areas by building  
732 new landforms, and influencing land use decisions in those locations (Nagabhatla et al., 2006;  
733 Ali and Narayana, 2015; Mageswaran et al., 2021).

Deleted: ,

Deleted: 6-

Deleted: ,

Deleted: .

Deleted: .

## 734 5.2 Inundation and run observation

735 Our computations have shown that the tsunami wave heights for around 5.5 m inundation 90  
736 m are observed in Bombooflat (Fig.4b). Similarly, the harbor area of Port Blair has seen  
737 structural failures in some building's foundations, and our computations show wave heights of  
738 3.6m in that area. Chidiya Tapu, which is 25 km from Port Blair, the estimated run-up is 3.9  
739 m, and the inundation is 585 m, which shows a gradual slope in the region, (Fig. 2). Coming to  
740 the Southpoint Magar area (Port Blair), a high run-up of 8.5 m is computed, and the inundation  
741 level is 550 m. Houses located near the open sea were completely washed away. At Wandoor  
742 Jetty in Port Blair, the calculated run-up is 3.46, the inundation is 450m, and the saltwater  
743 intrusion was observed due to the tsunami.

Deleted: 3 d). similarly

Deleted: harbour

Deleted: Figure No 2 i

Deleted: .

Deleted: runup

## 744 5.3 LULC vs economic change:

745 The presence of people, infrastructure, or assets in a hazard-prone location is referred to as  
746 exposure, and vulnerability is the degree to which a person, community, or system is  
747 susceptible to the impacts of a hazard. Vulnerability is determined by physical, social,  
748 economic, and environmental factors. (United Nations Office for Disaster Risk Reduction).  
749 Several factors can contribute to changes in exposure, such as population growth, Industrial  
750 development, and LULC change. It is anticipated that the population of the Andaman and  
751 Nicobar Islands will double by 2050 (Nanda and Haub, 2007), and the islands are experiencing  
752 an increasing influx of tourists. The increased population density in these regions intensifies  
753 the strain on already vulnerable lands. As a result, when a disaster, such as a natural calamity,

Deleted: Vulnerability

Deleted: a combination of

766 occurs in these areas, it affects the tourists and has severe repercussions for the large local  
767 population heavily dependent on tourism-related activities (Annan et al., 2005; Wood et al.,  
768 2019; Sathiparan et al., 2020, Hamuna et al., 2019). The increases in population from 1971 to  
769 2020, ~~as well as~~ built-up ~~areas, are~~ shown before and after the 2004 tsunami, and GSDP from  
770 2001 to 2020 in tsunami-prone areas of South Andaman are observed in Fig. 11.

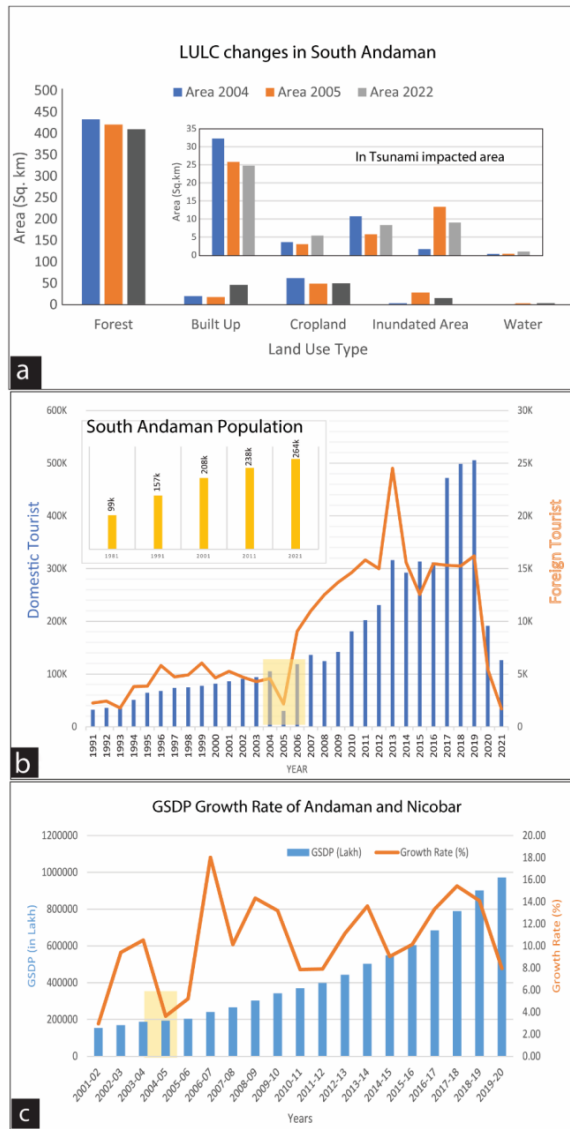
Deleted: .

Deleted: .

Deleted: and

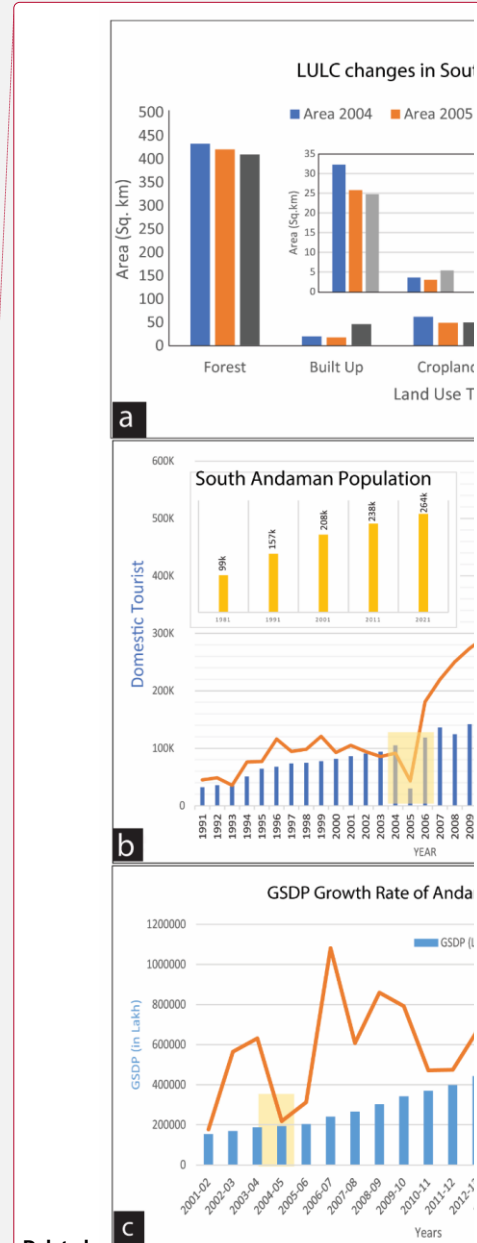
Deleted: area is

Deleted: 10



776

777 Figure 11 (a) LULC change in south Andaman and also in tsunami-affected areas of 2004. The LULC classification  
 778 reveals that there has been a significant increase in built-up areas, inundated areas, and water bodies, while the  
 779 agricultural land and vegetation have decreased. The increasing trends of tourists and local population in south  
 780 Andaman can be seen in Fig. (b). The GSDP growth rate shows the macroeconomic impact on GSDP in 2005 due  
 781 to the tsunami impact (c).



Deleted:

Deleted: 10

Deleted: and the

785 The increase in built-up areas could also positively impact the GSDP by boosting the  
786 construction and real estate sectors and providing more job opportunities in the tourism and  
787 hospitality industries, (Fig. 11a). The 2004 Indian Ocean tsunami significantly impacted the  
788 GSDP of the Andaman and Nicobar Islands, particularly in the tourism and fisheries industries,  
789 (Fig 11c). According to a report by the National Institute of Disaster Management, the  
790 Andaman and Nicobar Islands suffered losses amounting to INR 7.5 billion due to the 2004  
791 tsunami, with damages to the tourism industry being the most significant. It is important to  
792 carefully manage this growth and ensure sustainable development practices protecting both the  
793 natural environment and the local population's well-being. This includes implementing  
794 effective disaster preparedness measures, promoting sustainable tourism practices, and  
795 balancing economic development with environmental conservation in the region.

Deleted: .

Deleted: .

Deleted: of the local population

#### 796 5.4 Implication for changing scenario of vulnerability

797 India Inc. estimates that the total losses surpassed Rs 3,000 crore. Specifically, the losses in  
798 Andaman & and Nicobar Islands exceeded Rs 1,000 crore as per industry estimates  
799 (EconomicTimes.com). If a tsunami of similar magnitude were to occur again, the economic  
800 loss would be five times as high as those experienced in 2004. After the 2004 tsunami, the  
801 coastal area experienced significant development, with built-up areas expanding in already  
802 affected areas from ~7.38 % in 2004 to ~11.11 % in 2022. This increase in urbanization and  
803 infrastructure means that more properties, businesses, and critical facilities are now located in  
804 the coastal zone. The affected region's local population grew from 208k in 2001 to 264k in  
805 2021 (Figure 11b). With more people living in the coastal area, there is a higher risk of  
806 casualties and a greater demand for resources and aid during and after a tsunami. The number  
807 of tourists visiting the coastal area has increased significantly, from 98,000 tourists in 2001 to  
808 500,000 by 2019 (Figure 11b). Tourists are generally less familiar with local hazards and  
809 evacuation routes, making them more vulnerable during a tsunami. The presence of a large

Deleted: people

Deleted: people

Deleted: 10

Deleted: over the years. In 2001, there were

Deleted: , but by 2019, this number rose

Deleted: 10

819 number of tourists can add complexity to evacuation and relief efforts, potentially leading to  
820 higher economic losses. The region has experienced a sharp decline in forest and cropland  
821 areas. Forests act as natural buffers, helping to reduce the impact of a tsunami by absorbing  
822 some of the wave energy. Additionally, the loss of cropland can disrupt the supply chain during  
823 and after a disaster, affecting food availability and leading to economic losses beyond property  
824 damage.

## 825 6. Conclusions

826 The South Andaman region is vulnerable to tsunamis due to its location in the seismically  
827 active zone. In such an environment, tsunami preparedness and resilience are crucial. This  
828 includes implementing effective early warning systems, raising public awareness, and  
829 strengthening infrastructure resilience. Incorporating ecosystem-based approaches, such as  
830 preserving and restoring natural coastal land, can also contribute to reducing tsunami  
831 vulnerability. The South Andaman region is prone to shoreline changes due to natural processes  
832 and human activities. Regular monitoring and assessing these changes is crucial to  
833 understanding their impacts on coastal ecosystems and communities. Implementing  
834 appropriate coastal management strategies, such as beach nourishment, dune restoration, and  
835 erosion control measures, can help mitigate the negative effects of shoreline changes. It is  
836 important to adopt sustainable land use practices that balance economic development with  
837 resource conservation and responsible use. This involves promoting eco-friendly tourism,  
838 protecting sensitive ecosystems like mangroves and coral reefs, and implementing land use  
839 planning that considers the carrying capacity and vulnerability of the region. Tsunami modeling  
840 along the coastal locations shall help decision-makers how to construct structures along the  
841 coast. Decision makers will also be able to quantify the tsunami impact on sloping beaches,  
842 Flat beaches, and areas having boulders/mangroves. Engaging local communities,  
843 stakeholders, and indigenous knowledge holders in decision-making processes and promoting

**Deleted:** the preservation

**Deleted:** restoration of

**Deleted:** It is crucial to monitor

**Deleted:** assess

**Deleted:** regularly

**Deleted:** understand

**Deleted:** the

**Deleted:** of resources



852 capacity-building initiatives are critical for ensuring the sustainable development of the  
853 Andaman region.

854 **Code availability**

855 No

856 **Data availability**

857 All data included in this study are available upon request by contacting the corresponding  
858 author.

859 **Authors' contributions**

860 Vikas Ghadamode: Computations, Fieldwork, and Manuscript Writing.

861 K. Kumari Aruna: TUNAMI-N2 Computation and Fieldwork, Manuscript Writing

862 Anand Kumar Pandey: Manuscript Editing and Contribute Ideas and Suggestions

863 Kirti Srivastava: Paper Writing and TUNAMI-N2 Computations

864 **Competing interests / Conflicts of interest/**

865 The authors declare that they have no known conflicts of interest.

866 **Declarations**

867 The authors declare that they have no known conflicts of interest.

868 **Financial support**

869 No Funding

870 **Acknowledgements:**

871 The authors acknowledge encouragement and permission to publish from the Director, CSIR-

872 NGRI, ([NGRI/Lib/2024/Pub-51](#)). VG acknowledges UGC, India, for SRF for pursuing a PhD

873 (Grant no.: 10/UGC-JRF/209/19-ESTT).

874

Deleted: .

876 **References**

- 877 Ali, P. Y., & Narayana, A. C.: Short-term morphological and shoreline changes at Trinkat Island,  
878 Andaman and Nicobar, India, after the 2004 tsunami. *Marine Geodesy*,38(1), 26-39,  
879 <https://doi.org/10.1080/01490419.2014.908795> , 2015.
- 880 Annan, K.: *Reducing Risks from Tsunamis: Disaster and Development*. Nueva York: UNDP, 2005.
- 881 Bandopadhyay, P. C., & Carter, A.: Chapter 2 Introduction to the geography and geomorphology of the  
882 Andaman–Nicobar Islands. *Geological Society, London, Memoirs*, 47(1), 9-18,  
883 <https://doi.org/10.1144/M47.2>, 2017.
- 884 Bhat, G.R., Balaji, S. & Yousuf, M.: Tectonic geomorphology and seismic hazard of the east boundary  
885 thrust in northern segment of the Sunda–Andaman subduction zone. *Nat Hazards* 116, 401–423,  
886 <https://doi.org/10.1007/s11069-022-05680-6>, 2023.
- 887 Boak EH, Turner IL.: Shoreline definition and detection: a review. *J Coast Res* 21:688–703,  
888 <https://doi.org/10.2112/03-0071.1>, 2005.
- 889 Cho, Y. S., Lakshumanan, C., Choi, B. H., & Ha, T. M.: Observations of run-up and inundation levels  
890 from the teletsunami in the Andaman and Nicobar Islands: A field report. *Journal of Coastal*  
891 *Research*, 24(1), 216-223, <https://doi.org/10.2112/06-0662.1>, 2008.
- 892 Cooper JA, Jackson D, Nava F, McKenna J, Malvarez G.: Storm impacts on an embayed high energy  
893 coastline, western Ireland. *Marine Geol* 210:261–280,  
894 <https://doi.org/10.1016/j.margeo.2004.05.012>, 2004.
- 895 Crowell, M., Douglas, B. C., & Leatherman, S. P.: On forecasting future US shoreline positions: a test  
896 of algorithms. *Journal of Coastal Research*, 1245-1255, <http://www.jstor.org/stable/4298734>,  
897 1997.
- 898 Curry, J. R.: Tectonics and history of the Andaman Sea region. *Journal of Asian Earth Sciences*, 25(1),  
899 187-232, <https://doi.org/10.1016/j.jseaes.2004.09.001>, 2005.
- 900 Davis, R.A.: Human Impact on Coasts. In: Finkl, C.W., Makowski, C. (eds) *Encyclopedia of Coastal*  
901 *Science*. *Encyclopedia of Earth Sciences Series*. Springer, Cham, [https://doi.org/10.1007/978-3-](https://doi.org/10.1007/978-3-319-93806-6_175)  
902 [319-93806-6\\_175](https://doi.org/10.1007/978-3-319-93806-6_175), 2019.
- 903 Den Boer, E. L., & Oele, A. C.: Determination of shoreline change along the East-Java coast, using the  
904 Digital Shoreline Analysis System. In *MATEC Web of Conferences (Vol. 177, p. 01022)*. EDP  
905 Sciences, <https://doi.org/10.1051/mateconf/201817701022>, 2018.
- 906 Devi, E. U., & Sheno, S. S. C.: Tsunami and the effects on coastal morphology and ecosystems: a  
907 report. *Proceedings of the Indian National Science Academy*, 78(3), 513-521, 2012.
- 908 Dolan, R., Fenster, M. S., & Holme, S. J.: Temporal analysis of shoreline recession and accretion.  
909 *Journal of coastal research*, 723-744, <http://www.jstor.org/stable/4297888>, 1991.
- 910 Ghadamode, V., Srivastava, K., Singh, R. K., & Pandey, A. K.: Spatial analysis techniques for tsunami  
911 vulnerability and inundation mapping of Andaman region using remote sensing, GIS, AHP, and  
912 Fuzzy logic methods. *Environmental Earth Sciences*, 81(17), 427,  
913 <https://doi.org/10.1007/s12665-022-10548-w>, 2022.
- 914 Ghosh, T., Jana, P., Giritharan, S., Bardhan, S., Basir, S. R., & Roy, A. G.: Tsunami Survey in Andaman  
915 Nicobar Group of Islands. *Sumatra–Andaman Earthquake and Tsunami*, 26, 2004.

**Deleted:** Chen X.: Using remote sensing and GIS to analyse land cover change and its impacts on regional sustainable development. *Int J Remote Sens* 23(1):107–124, <https://doi.org/10.1080/01431160010007051>, 2002.¶

**Deleted:** <https://doi.org/10.1016/j.margeo.2004.05.012>, 2004.

922 Hamuna, B., Kalor, J. D., & Tablaseray, V. E.: The impact of tsunami on mangrove spatial change in  
923 the eastern coast of Biak Island, Indonesia. Journal of Ecological Engineering, 20(3),  
924 <http://dx.doi.org/10.12911/22998993/95094>, 2019.

925 Himmelstoss, E., Henderson, R. E., Kratzmann, M. G., & Farris, A. S.: Digital shoreline analysis system  
926 (DSAS) version 5.1 user guide (No. 2021-1091). US Geological Survey,  
927 <https://doi.org/10.3133/ofr20211091>, 2021.

928 Imamura, F.: Review of Tsunami Simulation with a Finite Difference Method. Long Waves Runup  
929 Models, 1996.

930 Imamura, F., & Imteaz, M. A.: Long waves in two-layers: governing equations and numerical model.  
931 Science of Tsunami Hazards, 13(1), 3-24,1995.

932 Jain, S. K., Murty, C. V. R., Rai, D. C., Malik, J. N., Sheth, A., & Jaiswal, A.: Effects of M9 Sumatra  
933 earthquake and tsunami of December 26, 2004. Current Science, 88(3), 357-359,  
934 <https://www.currentscience.ac.in/Volumes/88/03/0357.pdf>, 2005.

935 Jaman, T., Dharanirajan, K., & Rana, S.: Land use and Land cover Change detection and Its  
936 Environmental Impact on South Andaman Island, India using Kappa coefficient Statistical  
937 Analysis and Geospatial Techniques, 2022.

938 Jayakumar K, Malarvannan S.: Assessment of shoreline changes over the Northern Tamil Nadu Coast,  
939 South India using WebGIS techniques. J Coast Conserv. 20(6):477-487,  
940 <https://link.springer.com/article/10.1007/s11852-016-0461-9>, 2016.

941 Jevrejeva, S., Jackson, L., Riva, R., Grinsted, A., & Moore, J.: Sea level rise with warming above 2  
942 degree. In EGU General Assembly Conference Abstracts (p. 3637), 2017.

943 Joesidawati, M. I.: Shoreline change in Tuban district, East Java using geospatial and digital shoreline  
944 analysis system (DSAS) techniques. International Journal of Oceans and Oceanography, 10(2),  
945 235-246, 2016.

946 Kumar ST, Mahendra RS, Nayak S, Radhakrishnan K, Sahu KC.: Coastal vulnerability assessment for  
947 Odisha state, East coast of India. J Coast Res 26:523-534, <https://doi.org/10.2112/09-1186.1>,  
948 2010.

949 Kumari P, Jnaneswari K, Rao D, Sridhar D.: Application of remote sensing and geographical  
950 information system techniques on geomorphological mapping of coastal part of East Godavari  
951 district. Andhra Pradesh, India. Int J Eng Sci Tech 4:4296-4300,  
952 <https://link.springer.com/article/10.1007/s11069-016-2252>, 2012.

953 Leatherman, S. P.: Shoreline change mapping and management along the US East Coast. Journal of  
954 Coastal Research, 5-13, 2003.

955 Mageswaran, T., Sachithanandam, V., Sridhar, R., Mahapatra, M., Purvaja, R., & Ramesh, R.: Impact  
956 of sea level rise and shoreline changes in the tropical island ecosystem of Andaman and Nicobar  
957 region, India. Natural Hazards, 109, 1717-1741,  
958 <https://link.springer.com/article/10.1007/s11069-021-04895-3>, 2021.

959 Mansinha, L., and Smylie, D.E.: The displacements fields of inclined faults, Bull. Seismol. Soci. Am.,  
960 61(5), 1433-1440, 1971.

961 Mishra, P., Usha, T., & Ramanamurthy, M. V.: Evaluation of tsunami vulnerability along the northeast  
962 coast of India. Continental Shelf Research, 79, 16-22, 2014.

Deleted: coastal

Moved (insertion) [3]

Moved up [3]: V.

Deleted: Jangir, B., Satyanarayana, A. N. V., Swati, S., Jayaram, C., Chowdary,

Deleted: M., & Dadhwal, V. K.: Delineation of spatio-temporal changes of shoreline and geomorphological features of Odisha coast of India using remote sensing and GIS techniques. *Natural Hazards*, 82(3), 1437-1455, <https://link.springer.com/article/10.1007/s11069-016-2252>, 2016.¶

Deleted: <https://link.springer.com/article/10.1007/s11852-016-0461-9>.

975 Misra, A., & Balaji, R.: A study on the shoreline changes and Land-use/land-cover along the South  
 976 Gujarat coastline. *Procedia Engineering*, 116, 381-389,  
 977 <https://doi.org/10.1016/j.proeng.2015.08.311>, 2015.

978 Moran CAA.: Spatio-temporal analysis of texas shoreline changes using GIS technique. *Mediterranean*  
 979 *Mar Sci* 2:5–13, <https://hdl.handle.net/1969.1/408>, 2003.

980 Mukhopadhyay, A., Mukherjee, S., Hazra, S., & Mitra, D.: Sea level rise and shoreline changes: a  
 981 geoinformatic appraisal of Chandipur coast, Orissa. *Int J Geol Earth Environ Sci*, 1(1), 9-17,  
 982 2011.

983 Murali M, Ankitha M, Amritha S, Vethamony P.: Coastal vulnerability of Puducherry coast, India,  
 984 using analytical hierarchical process. *Nat Hazards Earth Syst Sci* 13:3291–3311,  
 985 <https://doi.org/10.5194/nhess-13-3291-2013>, 2013.

986 Nagabhatla, N., Roy, P. S., & Jagdale, R.: Evaluating the change (1968-2001) in landscape pattern and  
 987 analyzing disturbance in Baratang Forest Division (Andaman Islands), SOUTHEAST ASIA,  
 988 <https://hdl.handle.net/10568/40948>, 2006.

989 Nanda, A. R., & Haub, C.: The future population of India—a long-range demographic view. *Popul Res*  
 990 *Bureau*, 2007.

991 Natarajan, L., Sivagnanam, N., Usha, T., Chokkalingam, L., Sundar, S., Gowrappan, M., & Roy, P. D.:  
 992 Shoreline changes over last five decades and predictions for 2030 and 2040: a case study from  
 993 Cuddalore, southeast coast of India. *Earth Science Informatics*, 14(3), 1315-1325, 2021.

994 National Research Council: Tsunami warning and preparedness: an assessment of the US tsunami  
 995 program and the nation's preparedness efforts, Committee on the Review of the Tsunami Warning  
 996 and Forecast System and Overview of the Nation's Tsunami Preparedness, National Research  
 997 Council, 284 pp, 2011.

998 Nayak S.: Use of coastal data in coastal mapping. *Indian Carto CMMC* 147–156, 2002.

999 Raj, N., Rejin Nishkalank, R.A., Chrisben Sam, S.: Coastal Shoreline Changes in Chennai: Environment  
 1000 Impacts and Control Strategies of Southeast Coast, Tamil Nadu. In: Hussain, C. (eds) Handbook  
 1001 of Environmental Materials Management. Springer, Cham. https://doi.org/10.1007/978-3-319-  
 1002 58538-3\_223-1, 2020.

1003 Prabhbir Singh., and Kamlesh Khanduri.: Land use and Land cover change detection through Remote  
 1004 Sensing & GIS Technology: Case study of Pathankot and Dhar Kalan Tehsils. *Inter. Journal, of.*  
 1005 *Geomatics and Geosciences* 1(4), pp 839-846, 2011.

1006 Prerna, R., Srinivasa Kumar, T., Mahendra, R. S., & Mohanty, P. C.: Assessment of Tsunami Hazard  
 1007 Vulnerability along the coastal environs of Andaman Islands. *Natural Hazards*, 75, 701-726,  
 1008 <https://link.springer.com/article/10.1007/s11069-014-1336-8>, 2015.

1009 Ramalanjaona, G.: Impact of 2004 tsunami in the islands of Indian Ocean: Lessons learned. *Emergency*  
 1010 *Medicine International*, <https://doi.org/10.1155/2011/920813>, 2011.

1011 Rani, V. S., Srivastava, K., & Dimri, V. P.: Tsunami propagation and inundation due to tsunamigenic  
 1012 earthquakes in the Sumatra-Andaman subduction zone: Impact at Visakhapatnam. *Marine*  
 1013 *Geodesy*, 34(1), 48-58. https://doi.org/10.1080/01490419.2011.547802, 2011.

1014 Reguero, B. G., Beck, M. W., Agostini, V. N., Kramer, P., & Hancock, B., Coral reefs for coastal  
 1015 protection: A new methodological approach and engineering case study in Grenada. *Journal of*

**Deleted:** Mouat DA, Lancaster J.: Use of remote sensing and GIS to identify vegetation change in the upper San Pedro River watershed. *Arizona Geocarto Int* 11(2):55–67, <https://doi.org/10.1080/10106049609354534>, 1996.¶  
 Mujabar S, Chandrasekhar.: A shoreline change analysis along the coast between Kanyakumari and Tuticorin, India, using digital shoreline analysis system. *Geo-spatial Inf Sci* 14:282–293, <https://link.springer.com/article/10.1007/s12517-011-0394-4>, 2011.¶  
 Mujabar S, Chandrasekar N.: Shoreline change analysis along the coast between Kanyakumari and Tuticorin of India using remote sensing and GIS. *Arab J Geosci*. <https://doi.org/10.1007/s12517-011-0394-4>, 2011a.¶  
 Mujabar S, Chandrasekar N.: A Shoreline change analysis along the coast between Kanyakumari and Tuticorin, India using remote sensing and GIS. *Arab J Geosci* 6(2013):6647–6664, <https://link.springer.com/article/10.1007/s12517-011-0394-4>, 2011b.¶

**Deleted:** ocean

**Deleted:** <https://doi.org/10.1155/2011/920813>.

1038 [Environmental Management](https://doi.org/10.1016/j.jenvman.2018.01.024), 210, 146-161, <https://doi.org/10.1016/j.jenvman.2018.01.024>,  
1039 2018.

1040 Rowland, E. D., Lolade, A. A., Nicholas, D. O., Opukumo, A. W., & Omonefe, F.: The Environmental  
1041 Impact of Shoreline Changes and Land Use/Land Cover Change Detection in the Niger Delta  
1042 Region using Geospatial Technology. *Journal of Asian Scientific Research*, 12(4), 237-248,  
1043 2022.

1044 [Sachithanandam, V., Mageswaran, T., Ragavan, P., Mahapatra, M., Sridhar, R., Ramesh, R., & Mohan,  
1045 P. M.: Mangrove regeneration in tsunami-affected area of north and south Andaman using insitu  
1046 and remote sensing techniques, 2014.](#)

1047 [Sarkar, D., Mukhopadhyay, A., & Hazra, S.: Nature of tsunami and paleo tsunami deposits of South  
1048 Andaman. \*Int J Basic Appl Sci Res\*, 2\(3\), 2275-2285, 2012.](#)

1049 Sathiparan, N.: An assessment of building vulnerability to a tsunami in the Galle coastal area, Sri Lanka.  
1050 *Journal of Building Engineering*, 27, 100952, <https://doi.org/10.1016/j.jobbe.2019.100952>,  
1051 2020.

1052 Scheffers A, Scheffers S, Kelletat D.: Paleotsunami relics on the southern and central Antillean island  
1053 arc. *J Coast Res* 21:263–273, <https://doi.org/10.2112/03-0144.1>, 2005.

1054 Shaw, G., & Williams, A.: Impact of the Tsunami on the Tourism Industry and Ecosystem of the  
1055 Andaman and Nicobar Islands, India, 2006.

1056 Sheth, A., Sanyal, S., Jaiswal, A., & Gandhi, P.: Effects of the December 2004 Indian Ocean tsunami  
1057 on the Indian mainland. *Earthquake spectra*, 22(3\_suppl), 435-473,  
1058 <https://doi.org/10.1193/1.2208562>, 2006.

1059 [Singh, A. P., Murty, T. S., Rastogi, B. K., & Yadav, R. B. S.: Earthquake generated tsunami in the  
1060 Indian Ocean and probable vulnerability assessment for the east coast of India. \*Marine Geodesy\*,  
1061 35\(1\), 49-65, <https://doi.org/10.1080/01490419.2011.637849>, 2012.](#)

1062 Siva M.: Behera MR. Effect of continental slope on N-wave type tsunami run-up. *The International  
1063 Journal of Ocean and Climate Systems*, <https://doi.org/10.1177/1759313116656865>, 2016.

1064 South Andaman District – Population.: [https://www.census2011.co.in/census/district/53-south-  
1065 andaman.html](https://www.census2011.co.in/census/district/53-south-andaman.html). 2011-2023.

1066 [Srivastava, K., Begum, F., & Jakkula, M.: Tsunami Modelling and Run-ups along Indian Coasts.  
1067 \*Journal of the Geological Society of India\*, 97, 1307-1312, \[https://doi.org/10.1007/s12594-021-  
1861-5\]\(https://doi.org/10.1007/s12594-021-<br/>1068 1861-5\), 2021.](#)

1069 Sudha Rani NNV, Satyanarayana ANV, Bhaskaran PK.: Coastal vulnerability assessment studies over  
1070 India: a review. *Nat Hazards*, <https://link.springer.com/article/10.1007/s11069-015-1597>,  
1071 2015.

1072 Thakur, S., Dharanirajan, K., Ghosh, P. B., Das, P., & De, T. K.: Influence of anthropogenic activities  
1073 on the land use pattern of South Andaman Islands. *Research Journal of Marine Sciences*, 5(1), 1-  
1074 10, 2017.

1075 The Economic Times: [https://economictimes.indiatimes.com/tsunami-hits-india-inc-with-rs-3000-cr-  
1076 loss/articleshow/974281.cms?from=mdr](https://economictimes.indiatimes.com/tsunami-hits-india-inc-with-rs-3000-cr-loss/articleshow/974281.cms?from=mdr)

**Deleted:** environmental management

**Deleted:** Reid RS, Kruska RL, Muthui N, Taye A, Wotton S, Wilson CJ.: Land-use and land-cover dynamics in response to changes in climatic, biological and sociopolitical forces: the case of Southwestern Ethiopia. *Landscape Ecol* 15:339–355, <https://link.springer.com/article/10.1023/A:1008177712995>, 2000.¶

**Deleted:** Saraf AK, Choudhary PR.: Integrated remote sensing and GIS for ground water exploration and identification of artificial recharge sites. *Int J Remote Sens* 119:1825–1841, <https://doi.org/10.1080/014311698215018>, 1999.¶

**Deleted:** Siddiqui MN, Maajid S.: Monitoring of geomorphological changes for planning reclamation work in coastal area of Karachi, Pakistan. *Adv Space Res* 33:1200–1205, [https://doi.org/10.1016/S0273-1177\(03\)00373-9](https://doi.org/10.1016/S0273-1177(03)00373-9), 2004.¶

**Deleted:** <https://www.census2011.co.in/census/district/53-south-andaman.html>,

1097 Thieler ER, Himmelstoss EA, Zichichi JL, Ergul A.: Digital shoreline analysis system (DSAS) version  
1098 4.0-an ArcGIS extension for calculating shoreline change. US Geological Survey open-file report  
1099 2008–1278. US Geological Survey, Woods Hole, <https://doi.org/10.3133/ofr20081278>, 2009.

1100 Thiéblemont, R., Le Cozannet, G., Rohmer, J., Toimil, A., Álvarez-Cuesta, M., and Losada, I. J.: Deep  
1101 uncertainties in shoreline change projections: an extra-probabilistic approach applied to sandy  
1102 beaches, *Nat. Hazards Earth Syst. Sci.*, 21, 2257–2276, [https://doi.org/10.5194/nhess-21-2257-](https://doi.org/10.5194/nhess-21-2257-2021)  
1103 2021, 2021

1104 Tonisso H, Suursarr U, Kont A.: Maps, aerial photographs, orthophotos, and GPS data as a source of  
1105 information to determine shoreline changes, coastal geomorphic processes and their relation to  
1106 hydrodynamic conditions on Osmussa island, The Baltic sea. *IGRSS* 12:987–1159,  
1107 <https://doi.org/10.1109/IGARSS.2012.6350382>, 2012.

1108 Velmurugan, A., Swarnam, T. P., & Ravisankar, N.: Assessment of tsunami impact in South Andaman  
1109 using remote sensing and GIS. *J. Indian Soc. Remote Sensing*, 34(2), 193-202, 2006.

1110 Wood, N., Jones, J. M., Yamazaki, Y., Cheung, K. F., Brown, J., Jones, J. L., & Abdollahian, N.:  
1111 Population vulnerability to tsunami hazards informed by previous and projected disasters: a case  
1112 study of American Samoa. *Natural Hazards*, 95, 505-528,  
1113 <https://link.springer.com/article/10.1007/s11069-018-3493-7>, 2019.

1114 United Nations Office for Disaster Risk Reduction (UNDRR):  
1115 <https://www.preventionweb.net/understanding-disaster-risk/component-risk/vulnerability>,  
1116 2017.

1117 Yunus, A. P., & Narayana, A. C.: Short-term morphological and shoreline changes at Trinkat Island,  
1118 Andaman and Nicobar, India, after the 2004 tsunami. *Marine Geodesy*, 38(1), 26-39,  
1119 <https://doi.org/10.1080/01490419.2014.908795>, 2015.

1120 Yunus, A. P., Dou, J., Avtar, R., & Narayana, A.: Shoreline and coastal morphological changes induced  
1121 by the 2004 Indian Ocean tsunami in the Katchal Island, Andaman and Nicobar—a study using  
1122 archived satellite images. In *Tsunamis and earthquakes in coastal environments* (pp. 65-77).  
1123 Springer, Cham, [https://link.springer.com/chapter/10.1007/978-3-319-28528-3\\_5](https://link.springer.com/chapter/10.1007/978-3-319-28528-3_5), 2016.

1124 Yuvaraj, E., Saravanan, E., & Dharanirajan, K.: Assessment of land use and land cover changes in south  
1125 Andaman Island using remote sensing and GIS. *Int J Geomat Geosci*, 5, 171-181, 2014.

1126 Yi, L., Chen, J., Jin, Z., Quan, Y., Han, P., Guan, S., & Jiang, X.: Impacts of human activities on coastal  
1127 ecological environment during the rapid urbanization process in Shenzhen, China. *Ocean &*  
1128 *coastal management*, 154, 121-132, <https://doi.org/10.1016/j.ocecoaman.2018.01.005>, 2018.

1129

Deleted: U.S.

Deleted: U.S.

Deleted: Weng Q.: Land use change analysis in the  
Zhujiang Delta of China using satellite remote sensing,  
GIS, and stochastic modeling. *J Environ Manag* 64:273–28,  
<https://doi.org/10.1006/jema.2001.0509>, 2002.¶